เทคนิคที่เหมาะสมเพื่อลดการบิดเบือนของภาพดิฟฟิวชั่น ในคลื่นสะท้อนสนามแม่เหล็กไฟฟ้า 1.5 เทสล่า

นางสาวกนกวลี พลขนิษฐ์

วิทยานิพนธ์นี้เป็นส่วนหนึ่งของการศึกษาตามหลักสูตรปริญญาวิทยาศาสตรมหาบัณฑิต
สาขาวิชาฉายาเวชศาสตร์ ภาควิชารังสีวิทยา
คณะแพทยศาสตร์ จุฬาลงกรณ์มหาวิทยาลัย
ปีการศึกษา 2556

APPROPRIATE TECHNIQUE FOR REDUCE DISTORTION IN DIFFUSION WEIGHTED IMAGING MRI 1.5 TESLA

Miss Kanokvalee Ponkanist

A Thesis Submitted in Partial Fulfillment of the Requirements
for the Degree of Master of Science Program in Medical Imaging
Department of Radiology
Faculty of Medicine
Chulalongkorn University
Academic Year 2013

Thesis Title	APPROPRIATE TECHNIQUE FOR REDUCE DISTORTION IN DIFFUSION WEIGHTED IMAGING MRI 1.5 TESLA
By	Miss Kanokvalee Ponkanist
Field of Study	Medical Imaging
Thesis Advisor	Associate Professor Anchali Krisanachinda, Ph.D.
Thesis Co-Advisor	Associate Professor Sukalaya Lerdlum, M.D.
	Kitiwat Khamwan, Ph.D.

Accepted by the Faculty of Medicine, Chulalongkorn University in Partial Fulfillment of the Requirements for the Master's Degree

.....Dean of the Faculty of Medicine

(Associate Professor Sophon Napathorn, M.D.)

THESIS COMMITTEE

.....Chairman

(Assistant Professor Jarturon Tantivatana, M.D.)

.....Thesis Advisor

(Associate Professor Anchali Krisanachinda, Ph.D.)

.....Thesis Co-Advisor

(Associate Professor Sukalaya Lerdlum, M.D.)

.....Thesis Co-Advisor

(Kitiwat Khamwan, Ph.D.)

.....External Examiner

(Professor Franco Milano, Ph.D.)

กนกวลี พลขนิษฐ์ : เทคนิคที่เหมาะสมเพื่อลดการบิดเบือนของภาพดิฟฟิวชั่นในคลื่นสะท้อนสนามแม่เหล็กไฟฟ้า 1.5 เทสล่า. (APPROPRIATE TECHNIQUE FOR REDUCE DISTORTION IN DIFFUSION WEIGHTED IMAGING MRI 1.5 TESLA) อ.ที่ปรึกษาวิทยานิพนธ์หลัก: รศ. ดร.อัญชลี กฤษณจินดา, อ.ที่ปรึกษาวิทยานิพนธ์ร่วม: รศ. พญ.สุกัลยา เลิศล้ำ, ดร.กิติวัฒน์ คำวัน, 77 หน้า.

ภาพดิฟฟิวชั่นมีประโยชน์ในการวินิจฉัยโรคต่างๆ เช่น โรคสมองขาดเลือด โดยใช้เวลาในการทำสั้น. แต่เนื่องจากบริเวณส่วนฐานกระโหลกศีรษะมีส่วนประกอบของ โพรงอากาศ,กระดูกและเนื้อเยื่อ อยู่ติดกันทำให้เกิดความไม่สม่ำเสมอของสนามแม่เหล็ก ด้วยเหตุนี้ภาพของสมองในการทำดิฟฟิวชั่นจึงไม่มีความชัดเจนเกิดภาพบิดเบือน.วัตถุประสงค์ของงานวิจัยคือ เพื่อพิจารณาพารามิเตอร์ที่ลดความบิดเบือนของภาพดิฟฟิวชั่น ที่ใช้เทคนิคการ แสกนแบบ เอคโค่พลาน่า(Echo Planar Imaging: EPI) ในเครื่องถ่ายภาพสนามแม่เหล็กกำทอน 1.5 เทสลา โดยศึกษาในหุ่นจำลองแมกแฟนที่มีสารละลาย คอปเปอร์ซัลเฟตใส่ไว้เพียงครึ่งเดียวเพื่อจำลองสภาพการณ์ให้เหมือนกับบริเวณฐานกระโหลกศีรษะ การวิเคราะห์ค่าความบิดเบือนนี้วัดจากเทคนิคมาตรฐาน คือ เทอร์โบสปินเอคโค่ (Turbo Spin Echo: TSE) T2 และเทคนิคที่ใช้ในการทดลองได้แก่ EPI ที่ใช้แสกนร่วมและไม่ร่วมกับพารามิเตอร์ parallel image ซึ่งมี 2 แบบคือ GRAPPA และ mSENSE โดยทั้ง 2 แบบนี้จะมีการเพิ่มความเร็ว 2 หรือ 3 และวัดค่าความคลาดเคลื่อนทั้งใน b-value ทั้ง b0 และ b1000, หุ่นจำลองนี้จะมีอะคริลิคอยู่ทั้งหมด 3 กลุ่ม แต่ละกลุ่มจะประกอบด้วยอะคริลิค 5 จุด. หลังจากแสกนจากทั้ง 5 เทคนิคแล้ว หาตำแหน่งของจุดทั้งหมด และ หาความคลาดเคลื่อนเป็นเปอร์เซ็นต์เพื่อวิเคราะห์หาเปอร์เซ็นต์ความคลาดเคลื่อนของแต่ละตำแหน่ง โดยเปรียบเทียบกับการแสกนแบบเทอร์โบสปินเอคโค่ T2

จากการศึกษาสรุปได้ว่า EPI ที่ใช้ร่วมกับ GRAPPA และ mSENSE โดยใช้การเพิ่มความเร็วเป็น 2 , มีเปอร์เซ็นต์ความคลาดเคลื่อนลดลงจากEPI ที่ไม่ใช้ parallel image ประมาณ 50เปอร์เซ็นต์ และใน EPI ที่ใช้ร่วมกับ GRAPPA และ mSENSE โดยใช้การเพิ่มความเร็วเป็น 3 มีเปอร์เซ็นต์ความคลาดเคลื่อนลดลงมากกว่าการเพิ่มความเร็ว 2 แต่ในการใช้ EPI กับ mSENSE ที่มีการเพิ่มความเร็วเป็น 3 นั้นมีสัญญาณรบกวนจนไม่สามารถวัดค่าได้ใน b1000

ภาควิชา รังสีวิทยา
สาขาวิชา ฉายาเวชศาสตร์
ปีการศึกษา 2556

ลายมือชื่อนิสิต .....
ลายมือชื่อ อ.ที่ปรึกษาวิทยานิพนธ์หลัก .....
ลายมือชื่อ อ.ที่ปรึกษาวิทยานิพนธ์ร่วม .....
ลายมือชื่อ อ.ที่ปรึกษาวิทยานิพนธ์ร่วม .....

5574101830 : MAJOR MEDICAL IMAGING
KEYWORDS: MRI 1.5 TESLA / DIFFUSION WEIGHTED IMAGING / DISTORTION ARTIFACT REDUCTION / GRAPPA / MSENSE

KANOKVALEE PONKANIST: APPROPRIATE TECHNIQUE FOR REDUCE DISTORTION IN DIFFUSION WEIGHTED IMAGING MRI 1.5 TESLA. ADVISOR: ASSOC. PROF. ANCHALI KRISANACHINDA, Ph.D., CO-ADVISOR: ASSOC. PROF. SUKALAYA LERDLUM, M.D., KITIWAT KHAMWAN, Ph.D., 77 pp.

Diffusion Weighted Imaging (DWI) is an essential technique for diagnosis ischemic stroke, brain tumor in short scan time. At susceptibility area such as base of skull most distortion affects the image quality cause by in-homogeneity of magnetic field. The purpose of this study is to determine the scan parameters to reduce distortion artifact in MRI 1.5 Tesla Diffusion Weighted Imaging using EPI in MRI phantom. Methods: CuSO4 solution was filled half of Magphan phantom to represent base of skull, scan at tube support disk location using routine scan acquisition parameters.15 objects consist of 3 locations, 5 objects each were scanned. Measure and record co-ordinates(x,y) of each objects at 4 Echo Planar Imaging(EPI) with and without parallel image techniques (GRAPPA and mSENSE) and acceleration factor (R-factor) at 2 and 3 in b0 and b1000. Then compare the co-ordinates with Turbo Spin Echo T2 Technique (gold standard) and calculate the percent deviation.

In sequence EPI with GRAPPA and mSENSE R- factor 2, the percent deviation of each objects were lower than EPI without parallel around 50% in both b0 and b1000. Sequence EPI with GRAPPA and mSENSE R-factor 3 show more reduction. In b1000 of mSENSE more noise than GRAPPA was observed Discussion and Conclusion: The techniques EPI with GRAPPA and mSENSE R-factor 2 show reduce distortion artifact at susceptibility area such as base of skull. In EPI with GRAPPA and mSENSE R-factor 3 distortion was reduced more than R-factor 2, but more noise was observed in b1000.

Department:	Radiology	Student's Signature	.....
Field of Study:	Medical Imaging	Advisor's Signature	.....
Academic Year:	2013	Co-Advisor's Signature	.....
		Co-Advisor's Signature	.....

ACKNOWLEDGEMENTS

I would like to express gratitude and deepest appreciation to Associate Professor Anchali Krisanachinda, Ph.D., Department of Radiology, Faculty of Medicine, Chulalongkorn University, my advisor, for her guidance, helpful suggestion, supervision, constructive comments and polishing of the thesis writing to improve the English expression.

I am extremely grateful Associate Professor Sukalaya Lerdlum, M.D., Department of Radiology, Faculty of Medicine, Chulalongkorn University, for her advice and comments in the research.

I would like to extremely thank to Kitiwat Khamwan, Ph.D., Department of Radiology, Faculty of Medicine, Chulalongkorn University, for his advice and comments in the research.

I am extremely grateful Associate Professor Sivalee Suriyapee,M.Eng., Department of Radiology, Faculty of Medicine, Chulalongkorn University, my teacher for her invaluable advices, constructive comments.

I would like to extremely thank Mr.Taweap Sanghangthum, Ph.D., Mr. Sornjarod Oonsiri,M.Sc.,the Medical Physic staffs at Division of Radiation Oncology, Department of Radiology, King Chulalongkorn Memorial Hospital, for their invaluable advices, constructive comments.

I would like to deeply thank Professor Franco Milano, Ph.D. from University of Florence Italy, External examiner of this thesis defense for his helpful recommendations, constructive comments and teaching in Medical Imaging.

I would like to thank Mrs. Weeranuch Kitsukjit for her suggestion for the improvement.

Finally, I am extremely grateful for all teachers. Lectures and staffs at Master of Science in Medical Imaging, Faculty of Medicine, Chulalongkorn University for their help, and unlimited teaching during the course in Medical Imaging.

CONTENTS

Page

Page

Page

LIST OF TABLES

Page

Page

LIST OF FIGURES

Page

Page

CHAPTER I

INTRODUCTION

1.1Background and rationale

Magnetic resonance imaging (MRI) was firstly used as a tool for medical diagnosis in the latter part of the 20th Century. MRI has a wide range of applications in medical diagnosis with over 25,000 scanners in use worldwide (1) The main motivation for the MRI system is diagnostic, since MRI has not used any ionizing radiation in preference to CT when either modality could yield the same information. Even though MRI has much advantage but it still has downside in terms of artifacts such as chemical shift artifact, aliasing artifact, zipper artifact, susceptibility artifact etc. This study will focus on Diffusion Weighted Imaging (DWI) technique and determine parameters to reduce distortion artifact at susceptibility area.

Diffusion-weighted imaging (DWI) was developed 3 decades ago, with continuously improved to probe random microscopic motion of water protons on a per pixel basis. DWI techniques have advanced far beyond the experimental arena into routine clinical applications in ischemia and are also the subject of research in other diseases, such as multiple sclerosis, trauma (2, 3) The main motivation to adding DWI in conventional MRI brain sequence because shifts in the number of water protons between tissue compartments due to changes in permeability, osmolarity, or active transportation may occur in parallel. Ultimately, all these aspects will also have an impact on the extent of proton mobility(1).DWI needs short scan time to reduce the factor of flow such as vascular and cerebrospinal fluid (CSF) flow, mostly use Echo Planar Imaging (EPI)

Echo Planar Imaging (EPI) is achieved by means of rapid gradient switching, which maps all phase and frequency points in k-space during a single echo period. The major advantages of echo planar imaging over conventional image are (a) reduced imaging time with the potential for improved patient throughput, (b) reduced motion artifact, and (c) the ability to image rapid physiologic processes (4).

The general advantage of EPI is the fact that each profile in k-space acquires the same motion-induced phase error and k-space shift (1). Thus, in a magnitude reconstructed image these phase error terms are of no consequence. However, the maximum attainable spatial resolution of EPI can be markedly limited by T2*-decay during the long period of data acquisition. In addition, EPI has only a very small bandwidth per pixel along the phase encoding direction(5).

Hence, EPI is very susceptible to off-resonance effects, such as main field in-homogeneity, local susceptibility gradients, and chemical shift, which all may lead to severe image distortion. Typical regions which are affected by such artifacts are brain regions in the air cavities, such as around the posterior fossa, or nearby the nasal sinuses and the skull base(1).

1.2 Research Objective

To determine the scan parameters to reduce distortion artifact in MRI 1.5T Diffusion Weighted Imaging using EPI in MRI phantom.

CHAPTER II

REVIEW OF RELATED LITERATURE

2.1 Theory

2.1.1 The introduction of MRI

Nuclear Magnetic Resonance (NMR) was discovered in bulk matter in the 1950s and for many years its major application was in the field of spectroscopy; discerning chemical species from the inherent shift in resonant frequency exhibited by nuclei which depends on their chemical environment. It was not until the 1970s when Lauterbur introduced the concept of magnetic field gradients. That an image based on magnetic resonance could be produced By the 1980s whole body magnets were being produced in England permitting the first in vivo images of human anatomy. Currently the technique known as MR imaging, is wide spread and an estimated 20 million scans are performed worldwide each year. MR images with excellent soft-tissue contrast can be acquired in any imaging plane, and like CT it does not involve the use of ionizing radiation. It is the imaging modality of choice in brain and spinal cord which is routinely used in many other clinical settings (6).

Magnetic resonance imaging (MRI) has provided high temporal, spatial, and contrast resolution methods to assess structure. However, the need to assess beyond the purely anatomic aspects, such as biochemistry and tissue physiology, required the development of functional techniques such as functional magnetic resonance imaging (fMRI), perfusion weighted imaging (PWI), Diffusion Weighted Imaging (DWI) and magnetic resonance spectroscopy (MRS).

In selecting pulse sequences and measurement parameters for a specific application, MRI allows tremendous flexibility to produce variation contrast between normal and disease tissues as well as flowing blood for example: technique bright-blood and dark-blood. A typical patient examination acquires sets of images with multiple types of contrast (proton density, T1, T2) and multiple slice orientations (transverse, sagittal, coronal, and oblique) providing the clinician with more complete information on the nature of the tissue under observation and increasing the likelihood of lesion detection. It is important that the MR examinations be tailored to the organ or organs under investigation, the type of disease process, and the individual patient. The MR physician may choose to provide detailed measurement parameters for each examination, or have a predetermined regimen of scans performed by a technologist. Establishing fixed measurement protocols to ensure reliable, reproducible imaging examinations are performed.

2.1.2 Resonance and Relaxation

Nuclei with an odd number of protons and neutrons possess a property called spin. In quantum mechanics spin is represented by a magnetic spin quantum number. Spin can be

visualized as a rotating motion of the nucleus about its own axis. As atomic nuclei are charged, the spinning motion causes a magnetic moment in the direction of the spin axis. The strength of the magnetic moment is a property of the type of nucleus. Hydrogen nuclei (^{1}H), as well as possessing the strongest magnetic moment, are in high abundance in biological material. Consequently hydrogen imaging is the most widely used in MRI procedure. Consider a collection of 1H nuclei (spinning protons) as in Figure 2.1. In the absence of an externally applied magnetic field, the magnetic moments have random orientations. However, if an externally supplied magnetic field B_0 is imposed, the magnetic moments have a tendency to align with the external field (7).

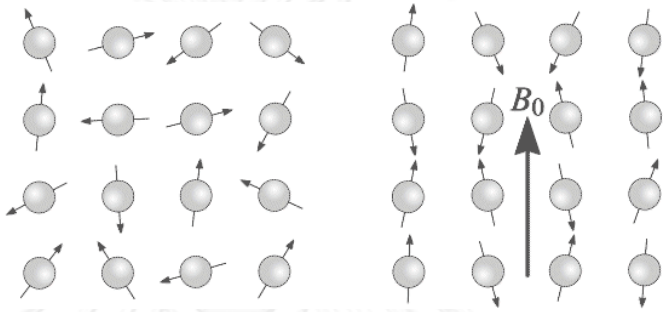

Figure 2.1 Two possible orientations for the proton in an external magnetic field.

The magnetic moments or spins are constrained to adopt one of two orientations with respect to B_0, denoted parallel and anti-parallel. The angles subtended by these orientations and the direction of B_0 are labelled theta in Figure 2.2(a). The spin axes are not exactly aligned with B_0, they precess around B_0 with a characteristic frequency as shown in Figure 2.2(b). This is analogous to the motion of a spinning top precessing in the earth's gravitational field. Atomic nuclei with the same magnetic spin quantum number as ^{1}H will exhibit the same effects - spins adopt one of two orientations in an externally applied magnetic field. Elements whose nuclei have the same magnetic spin quantum number include ^{13}C, ^{19}FE and ^{31}P. Nuclei with higher magnetic spin quantum number will adopt more than two orientations.

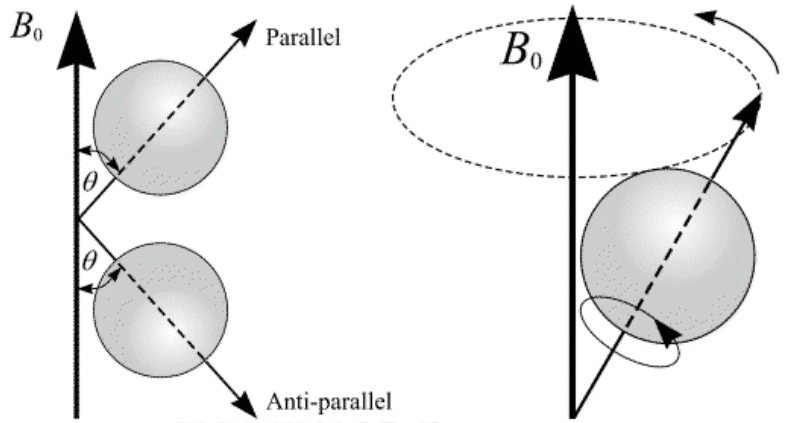

Figure 2.2 (a) In the presence of an externally applied magnetic field, B_0, nuclei are constrained to adopt one of two orientations with respect to B_0 (b) A magnetic moment precessing around B_0.

The Larmor equation expresses the relationship between the strength of a magnetic field, B_0, and the precessional frequency, F, of an individual spin.

$$\gamma B_0 = F.$$

The proportionality constant to the left of B_0 is known as the gyromagnetic ratio (γ) of the nucleus. The precessional frequency, F, is also known as the Larmor frequency. For a hydrogen nucleus, the gyromagnetic ratio is 4257 Hz/Gauss. Thus at 1.5 Tesla (15,000 Gauss), F = 63.855 Megahertz.

Radiofrequency field and MR signal (7): For a collection of ^{1}H nuclei, let the number of spins adopting the parallel and anti-parallel states be P1 and P2 respectively, with corresponding energy levels E1 and E2. E2 is greater than E1 causing P1 to be greater than P2.The reason that the spins adopt the higher energy anti-parallel state is that spins of P2 may move to P1 if the exact amount of energy, Δ(E) = E2 - E1 is supplied to the system. If the temperature of the system is absolute zero, all spins would adopt the parallel orientation.

At any given instant, the magnetic moments of a collection of ^{1}H nuclei can be represented as vectors, as shown in Figure 2.3. Every vector can be described by its components perpendicular to and parallel to B_0. For a large enough number of spins distributed on the surface of the cone, individual components perpendicular to B_0 cancel, leaving only components in the direction parallel to B_0. As most spins adopt the parallel rather than the anti-parallel state, the net magnetization M is in the direction of the B_0 field.

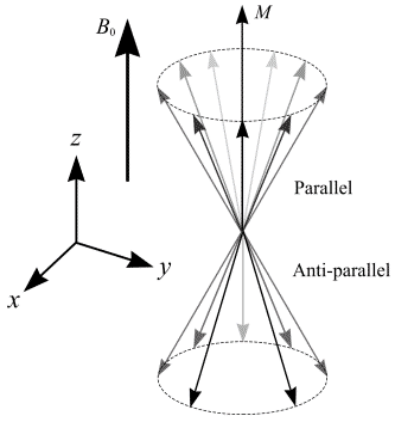

Figure 2.3 A collection of spins at any given instant in an external magnetic field, B_0. A small net magnetization, M, is detectable in the direction of B_0 (7).

Suppose the direction of B_0 is aligned with the z-axis of Euclidean 3-space. The plane perpendicular to B_0 contains the x and y-axes. In order to detect a signal from ^{1}H nuclei, radio frequency (RF) energy must be applied. RF energy at the Larmor frequency causes nuclear spins to swap between parallel and anti-parallel states. This has an oscillatory effect on the component of M parallel to the z-axis. RF energy, like all electromagnetic radiation, has electric and magnetic field components. Suppose the magnetic field component is represented by B_1 and lies in the x-y plane. The x-y components of M will be made coherent by the B_1 field giving a net x-y component to M and hence effectively causes M to tilt from the z direction into the x-y plane. This phenomenon is described further in Figure 2.4.

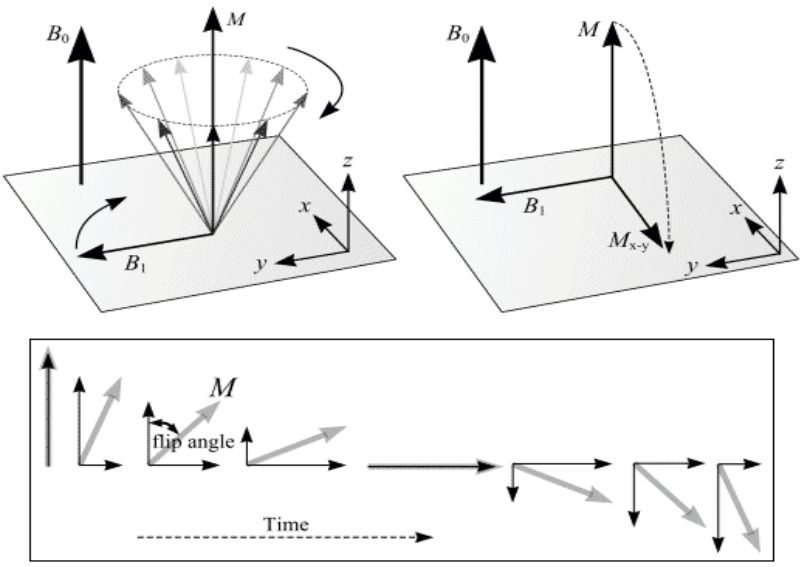

Figure 2.4 The effect of RF radiation on the net magnetization M to produce a second magnetic field M x-y. (bottom) Flip angle, through which M rotated away from the z-axis.

The angle through which M has rotated away from the z-axis is known as the flip angle. The strength and duration of B_1 determine the amount of energy available to achieve spin transitions between parallel and anti-parallel states. Thus, the flip angle is proportional to the strength and duration of B_1. After pulses of 90 degrees and 270 degrees, M has no z component and the population ratio P2:P1 is exactly one. A pulse of 180 degrees rotates M into a position directly opposite to B_0, with greater numbers of spins adopting anti-parallel (rather than parallel) states. If the B_1 field is applied indefinitely, M tilts away from the z-axis, through the x-y plane towards the negative z direction, and finally back towards the x-y plane and z-axis (where the process begins again).

The situation after an RF pulse is applied that causes the net magnetization vector M to flip by 90 degrees (figure 2.5a). M lies in the x-y plane and begins to precess about the B_0 axis. M will induce an electromotive force in a receiver coil according to Faraday's law of magnetic induction. This is the principle of NMR signal detection. It is from this received RF signal that an MR image can be constructed. Figure 2.5(b) shows a graph of the voltage or signal induced in a receiver coil verses time. Such a graph, or waveform, is termed a free induction decay (FID). The magnitude of the generated signal depends on the number of nuclei contributing to produce the transverse magnetization and on the relaxation times. The relaxation process can b divided into two parts: T1 and T2 relaxation (7).

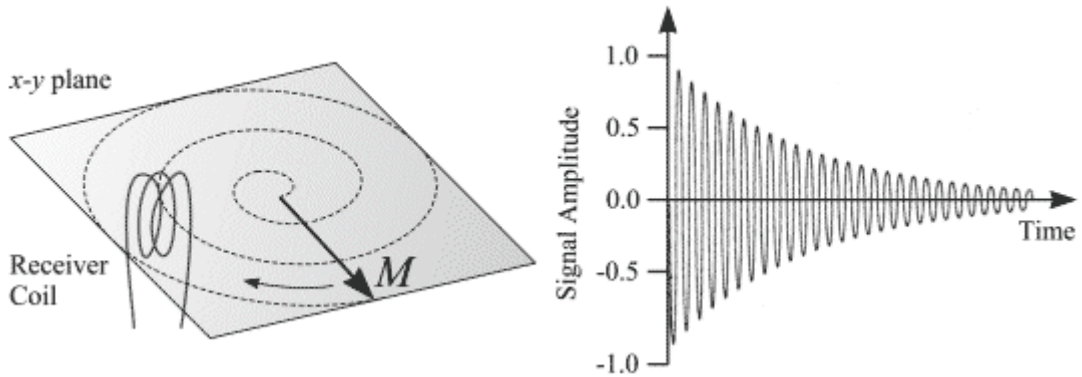

Figure 2.5 RF pulse applied to M and graph of signal induced in receiver coil

(a) After a 90 degrees RF pulse, M lies in the x-y plane and rotates about the z-axis. The component of M in the x-y plane decays over time. An alternating current, shown in

T1 Relaxation (8)

The T1 relaxation time, also known as the **spin-lattice relaxation time**, is a measure of how quickly the net magnetization vector recovers to ground state in the direction of B_0. The return of excited nuclei from the high energy state to the low energy or ground state is associated with loss of energy to the surrounding nuclei. Nuclear magnetic resonance was originally used to examine solids in the form of lattices, hence the name "spin-lattice" relaxation.

T1 relaxation is an exponential process as shown in the figure to the right. The length of the net magnetization vector for a spin echo sequence is given by the following equation:

$$M_t = M_{max}(1\text{-}e^{-t/T1})$$

where M_t is the magnetization at time = t, the time after the 90°pulse, M_{max} is the maximum magnetization at full recovery

At a time equals one T1, the signal will recover to 63% of its initial value after the RF pulse has been applied. After two T1 times, the magnetization is at 86% of its original length. Three T1 times gives 95%. Spins are considered completely relaxed after 3-5 T1 times.

T1 relaxation rate is the reciprocal of the T1 time (1/T1). T1 relaxation is fastest when the motion of the nucleus (rotations and translations or "tumbling rate") matches that of the Larmor frequency. As a result, T1 relaxation is dependent on the main magnetic field strength that specifies the Larmor frequency. Higher magnetic fields are associated with longer T1 times.

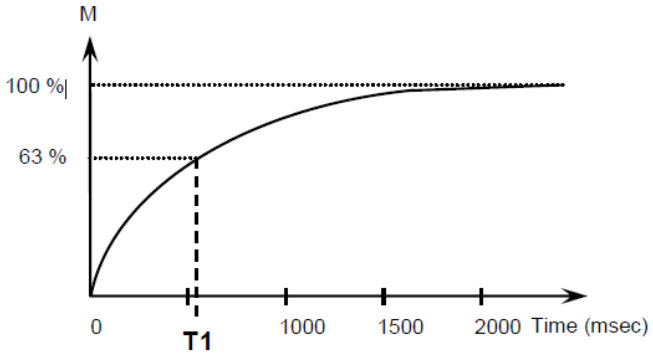

Figure 2.6 T1 relaxation

The curve shows at time 0 there is no magnetization in the Z-direction right after the RF-pulse. But immediately the M_z starts to recover along the Z-axis. T1 relaxation is a time constant. T1 is defined as the time it takes for the longitudinal magnetization (M_z) to reach 63 % of the original magnetization.

T2 relaxation(8)

T2 relaxation refers to the progressive dephasing of spinning dipoles following the 90° pulse as seen in a spin-echo sequence due to tissue-particular characteristics, primarily those that affect the rate of moment of protons, most of which are found in water molecules. This is alternatively known as spin-spin relaxation.

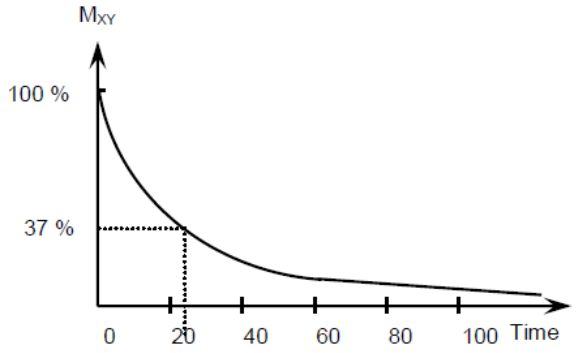

Figure 2.7 T2 relaxation(9)

The curve show T2 relaxation curve after the 90° RF-pulse all the magnetization is "flipped" into the XY-plane. The net magnetization is called M_{XY}. At time 0, all spins are in-phase, but immediately start to de-phase. T2 relaxation is also a time constant. T2 is defined as the time it takes for the spins to de-phase to 37% of the original value. The rate of de-phasing is different for each tissue. Fat tissue will de-phase quickly, while water will de-phase much slower

2.1.3 Spatial Encoding

The appearance of images is in terms of brightness or contrast and with the digital nature of the image, as pixels or voxel. The image-formation process is particularly helpful for obtaining the optimum diagnostic information from an examination, modifying or creating new protocols, recognizing common image artifacts and taking measures to overcome or avoid them. Anatomy of a pulse sequence: particularly spin echo, may take a long time to acquire, that the progress of the scan involves a loud banging sound from the MR system and that sometimes there is more silence than banging. Each sound is produced by *gradient* pulses applied to interrogate every possible spatial frequency that may contribute to the image. In MR the static magnetic field B_0 is constantly present the gradients are not. They are applied in a controlled fashion to form an MR *pulse sequence*. MR pulse sequences do a number of things; however, in this chapter we will only consider a basic gradient-echo pulse sequence from the point of view of how it manages to localize the MR signal. An MR pulse sequence diagram is a simple means of showing how the RF and gradients are applied. The vertical axis represents amplitude and the horizontal axis is time. Figure 2.8 shows a basic gradient-echo MR imaging sequence (10).

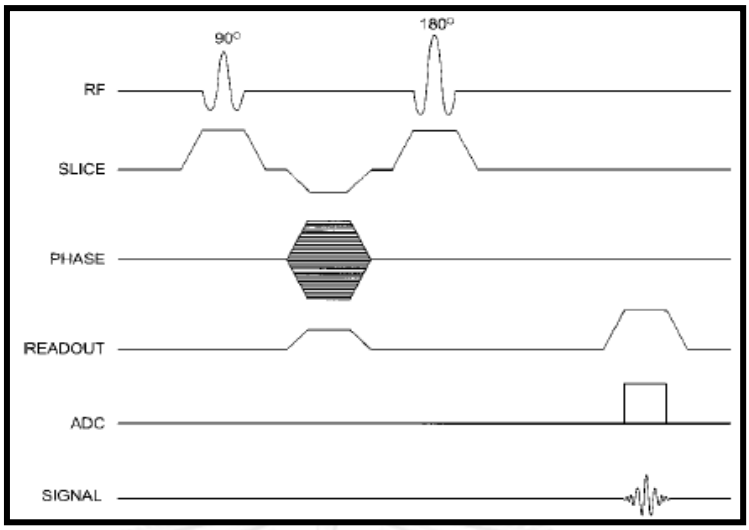

Figure 2.8 Spin echo diagram (7)

First (top line) an RF pulse is applied simultaneously with a slice-selective gradient *G*SS (line 2). The RF pulse stimulates the MR interactions in tissue which lead to the MR signal. By combining the RF excitation with a gradient the MR interactions are restricted to a two-dimensional plane, slab or slice. Any physical gradient *G*x, *G*y or *G*z or combinations of these can be used for this purpose, allowing us to produce transverse, sagittal or coronal, oblique or double oblique slices. Next, in line 3, *phase encoding* is applied in a direction orthogonal to the slice selection. This encodes the MR signal in the phase-encode direction. In line 4, the *frequency-encode* or readout gradient is applied in the third direction and finally line 5 shows the time when the MR signal is measured or *acquired*. Note that this is during the frequency-encoding gradient until the data or *k-space* matrix is filled. A time period, TR, occurs between the application of one RF excitation and the next. The total scan time is the product of NSA, N_{PE} and TR

$$\text{Scan time} = \text{NSA} \times N_{PE} \times \text{TR}$$

where NSA is the number of signal averages and N_{PE} the size of the phase-encoding matrix. Once all the data are acquired a two-dimensional Fourier transform is applied. This converts the data, already encoded as spatial frequencies, into an image. Reconstruction in MRI is generally simpler than in X-ray CT; most of the hard work has been done during the acquisition by the gradients.

2.1.4 Frequency Encoding

The frequency encoding gradient is turned on just before the receiver is gated on and is left on while the signal is sampled or read out. For this reason the frequency encoding gradient is also known as the readout gradient. The resulting FID is a graph of signal (formed from the

interference pattern of the different frequencies) induced in the receiver versus time. If the FID is subjected to Fourier transform, a conventional spectrum in which signal amplitude is plotted as a function of frequency can be obtained. Thus, a graph of signal versus frequency is obtained which corresponds to a series of lines or views representing columns of spins in the slice. Figure 2.9 shows two simple FIDs and their Fourier transforms (7).

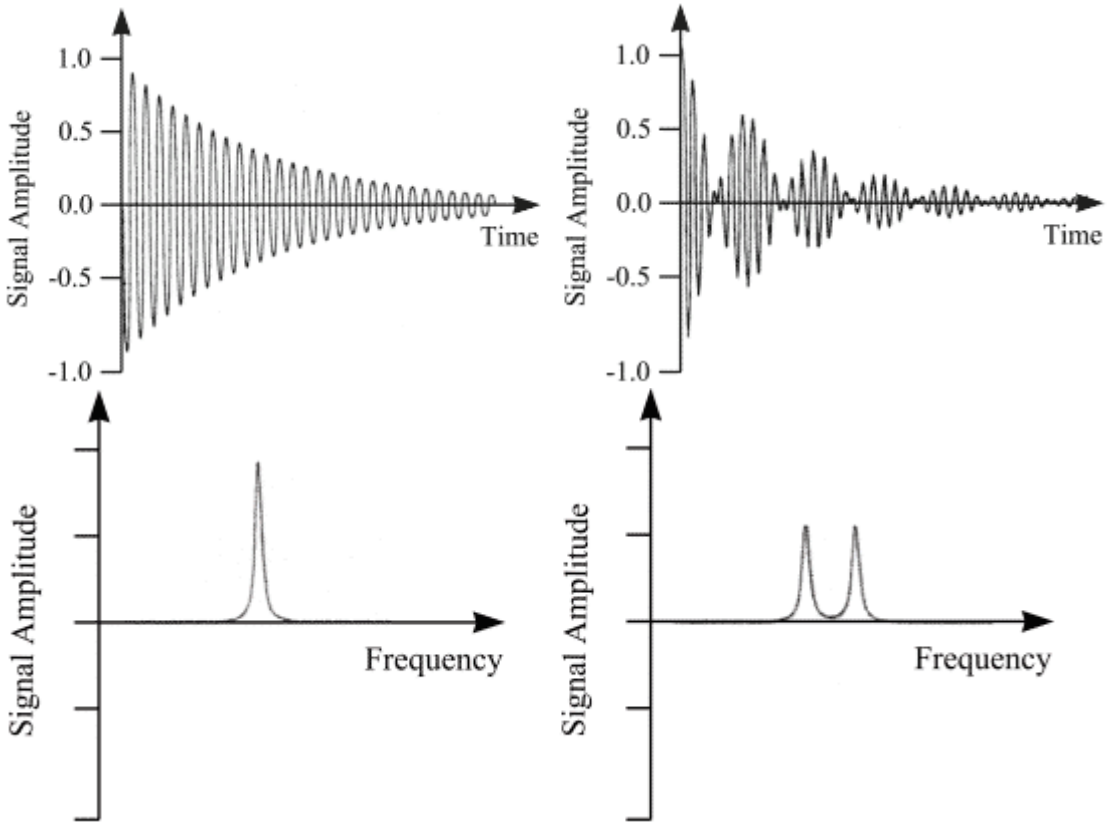

Figure 2.9 Two FIDs and their Fourier transforms

2.1.5 Phase Encoding

A phase encoding gradient is applied orthogonally to the other two gradients after slice selection and excitation, but before frequency encoding. The phase encoding gradient does not change the frequency of the received signal because it is not on during signal acquisition. It serves as a phase memory, remembering relative phase throughout the slice.

To construct a 256 x 256 pixel image a pulse sequence is repeated 256 times with only the phase encoding gradient changing. The change occurs in a stepwise fashion, with field strength decreasing until it reaches zero, then increasing in the opposite direction until it reaches its original amplitude. At the end of the scan, 256 lines (one for each phase encoding steps) comprising 256 samples of frequency are produced. A Fourier transformation allows phase information to be extracted so that a pixel (x, y) in the slice can be assigned the intensity of

signal which has the correct phase and frequency corresponding to the appropriate volume element (7).

2.1.6 MRI Sequences

Spin Echo Pulse Sequence (7): The spin echo (SE) sequence is the most commonly used pulse sequence in clinical imaging. The sequence comprises two radiofrequency pulses - the 90 degree pulse that creates the detectable magnetization and the 180 degree pulse that refocuses it at TE. The selection of TE and TR determines resulting image contrast. In T1-weighted images, tissues that have short T1 relaxation times (such as fat) present as bright signal. Tissues with long T1 relaxation times (such as cysts, cerebrospinal fluid and edema) show as dark signal. In T2-weighted images, tissues that have long T2 relaxation times (such as fluids) appear bright.

In cerebral tissue, differences in T1 relaxation times between white and grey matter permit the differentiation of these tissues on heavily T1-weighted images. Proton density-weighted images also allow distinction of white and grey matter, with tissue signal intensities mirroring those obtained on T2-weighted images. In general, T1-weighted images provide excellent anatomic detail, while T2-weighted images are often superior for detecting pathology.

Gradient Recalled Echo Pulse Sequences (7): Gradient Echo or Gradient recalled echo (GRE) sequences, which are significantly faster than SE sequences, differ from SE sequences in that there is no 180 degree refocusing RF pulse. In addition, the single RF pulse in a GRE sequence is usually switched on for less time than the 90 degree pulse used in SE sequences. The scan time can be reduced by using a shorter TR, but this is at the expense of the signal to noise ratio (SNR) which drops due to magnetic susceptibility between tissues. At the interface of bone and tissue or air and tissue, there is an apparent loss of signal that is heightened as TE is increased. Therefore it is usually inappropriate to acquire T2-weighted images with the use of GRE sequences. Nevertheless, GRE sequences are widely used for obtaining T1-weighted images for a large number of slices or a volume of tissue in order to keep scanning times to a minimum. GRE sequences are often used to acquire T1-weighted 3D volume data that can be reformatted to display image sections in any plane. However, the reformatted data will not have the same in-plane resolution as the original images unless the voxel dimensions are the same in all three dimensions.

Inversion Recovery (10): Inversion Recovery is a magnetization preparation technique followed by an imaging sequence of the spin echo type in its standard version. The sequence starts with a 180° RF inversion wave which flips longitudinal magnetization M_z in the opposite direction. Due to longitudinal magnetization will increase to return to its initial value, passing through null value. To measure the signal, a 90° RF wave is applied to obtain transverse magnetization. The delay between the 180° RF inversion wave and the 90° RF excitation wave is referred to as the inversion time TI. As longitudinal regrowth speed is characterized by relaxation time T1, these sequences are weighted in T1. Inversion-recovery also increases weighting of

associated imaging sequence (spin echo or gradient echo of varying speeds). With this type of sequence; certain tissues have a negative signal in terms of display, two possibilities exist.

Either signal magnitude (amplitude in relation to 0) used for gray scale display: the gray levels will be distributed from the negative signal values to the positive values (with a null signal background that will be gray rather than black): this is the (true) display type. Another property of inversion-recovery sequences is linked to choice of TI. If a TI is chosen such that the longitudinal magnetization of a tissue is null, the letter cannot emit a signal (absence of longitudinal magnetization).The inversion-recovery technique thus allows the signal of a given tissue to be supposed by selecting a TI adapted to the T1 of this tissue. Inversion-recovery can be combined with sequence types other than the standard spin echo. In particular, it can be used with fast spin echo sequences, to save considerable time, as inversion-recovery requires relatively long TR to allow magnetization the time to regrow, Inversion also serves as magnetization preparation for gradient echo sequences, to weight them in T1.

2.1.7 Fourier transforms

Fourier transforms: Joseph Fourier was a French mathematician who enjoyed a colorful life spanning science, politics and high society during the time of the Emperor Napoleon Bonaparte. His lasting achievement was the invention of the Fourier transform, a concept which met with much resistance from the scientific establishment of his time, but one which entirely underpins the theory of MR imaging. Fourier's great idea was that any signal or waveform in time could be split up into a series of 'Fourier components' each at a different frequency. For example, the sound of a musical instrument could be described either by the actual pressure waveforms it produced in *the time domain*, or by the appropriate magnitude of its constituent frequencies or its *spectrum* in the *frequency domain*. An acoustic signal, such as that produced by a musical instrument, is an example of a one dimensional waveform and when Fourier transformed gives a one-dimensional spectrum. In MR we use two or three-dimensional Fourier transforms. Variables which relate to each other in their respective domains are called Fourier transform pairs. One of the key features of the Fourier transform is that 'less is more': if a shape is small in one domain, its transform will be large in the other.

2.1.8 MR equipment

Magnets: The magnet is the main component of the MR system. Due to design constraints the static magnetic field is inherently non-uniform and its *homogeneity* is optimized by a process known as shimming whereby pieces of steel and/or electrical coils are incorporated into the magnet to improve the uniformity over a given volume. This process is usually performed at system installation; however, many systems give the user limited ability to improve

the homogeneity on a per-patient basis during scan set-up. This is particularly import ant for techniques such as fat suppression, steady state imaging or spectroscopy.

A magnet will also generate a magnetic field outside of the patient aperture. Considerable effort is invested in designing magnets whereby the extent of this *fringe field* is minimized. However, for some sites additional magnetic field shielding may be required either for safety reasons or to avoid interference with nearby sensitive electronic components.

Magnetic field strength is measured in tesla (T). Whole-body magnets have been constructed with field strengths of 0.02–8 T. Typical clinical systems operate in the range of 0.2–3.0 T. Spectroscopy is generally performed at 1.5 T and above. The advantages of higher field strengths are a better SNR and increased chemical shift effects, improving spectral fat suppression and spectroscopy. The improvement in SNR with increasing field strength may be traded for increased spatial resolution, or decreased imaging time.

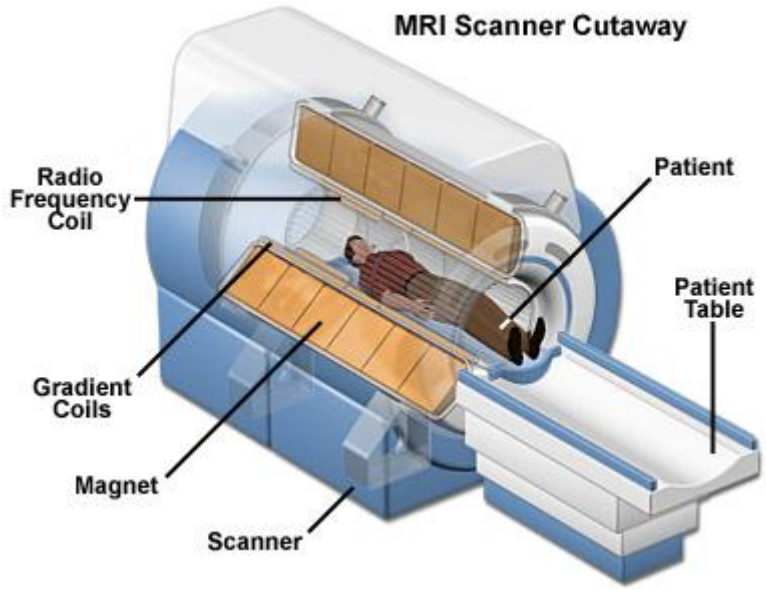

Figure 2.10 Components in a typical MR system (11)

Gradients: The gradient coils mounted on a cylindrical transformer just inside the bore of the magnet. In a standard cylindrical magnet, such as a superconducting system, the direction along

the bore is termed the *z* axis, the left–right direction is termed the *x* axis and the top–bottom direction is termed the *y* axis. Although the gradients are oriented in the three orthogonal directions, the gradient magnetic fields themselves are parallel to the main magnetic field B_0. The null point at the centre of the gradient coils, and also the centre of the magnet, is called the *isocentre*.

The *z* gradient (G_z) can be generated through the use of a single pair of coils with counter-rotating currents known as a Maxwell pair shown in figure 2.10 The optimum gradient

linearity occurs when the coils are separated by $r\sqrt{3}$, where r is the coil radius. Other designs can generate z gradients with much better radial linearity, e.g. spiral windings with variable pitch along the z axis.

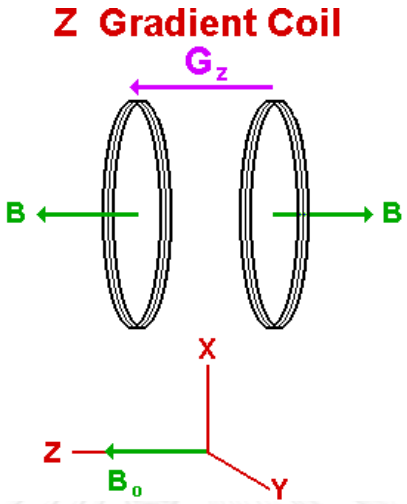

Figure 2.11 Maxwell pair configuration for a longitudinal (Z) gradient field (12)

X axis and Y axis gradients G_y can be generated using the Golay configuration shown in figure 2.11 comprising four coils on the surface of the cylindrical former with the currents producing a quadrupolar magnetic field (i.e. one having two North and two South poles). Only the innermost arcs contribute usefully to producing a transverse gradient with the field parallel to B_0. The G_x gradient can be generated using an identical set of Golay coils rotated through 90°.

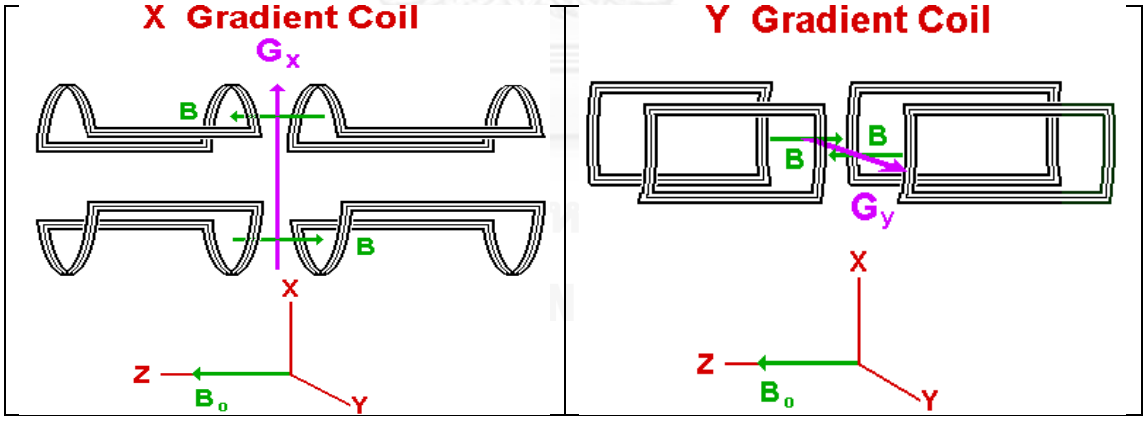

Figure 2.12 Golay coils configuration for transverse(x and y) gradient fields(12).

Radiofrequency systems: The radiofrequency (RF) system comprises a transmitter, coil and receiver. The purpose of the transmitter is to generate suitably shaped pulses of current at the Larmor frequency. When this current is applied to the coil an alternating B field is produced. The coil will also detect the MR signal from the patient. The frequency-encoding process will result in a narrow range of useful frequencies, e.g. _16 kHz, centered at the Larmor frequency. It is the function of the receiver to remove, or more correctly demodulate, this _16 kHz range of

interest from the much higher (Larmor frequency) The transmitter has to generate RF pulses with appropriate centre frequencies, bandwidths, amplitudes and phases in order to excite nuclei within the desired slices or slabs. The slice position and the strength of the slice select gradient at that location determine the centre frequency of the pulse. The bandwidth, or the range of frequencies within the pulse, controls the thickness of the excited slice. The shape and duration of the RF pulse envelope determines the bandwidth. The amplitude of the RF pulse controls how much the magnetization is flipped by the pulse, whilst the phase controls along which axis the magnetization is flipped (in the rotating frame of reference). In modern MRI systems the RF pulse envelope is generated digitally.

The receiver coil maximizes signal detection, whilst minimizing the noise. Usually the major source of noise is from the patient's tissue (from the Brownian motion of electrolytes). To minimize the noise, and maximize the SNR, it is necessary to minimize the coil dimensions, i.e. the coil's volume should be filled as much as possible by the sample. A compromise needs to be made between adequate RF homogeneity and high SNR. There are two types of receiver coil: volume and surface. Volume coils completely encompass the anatomy of interest and are often combined transmit/receive coils. Surface coils are generally received only, due to their inhomogeneous reception field. They are however, as their name suggests, good for detecting signal near the surface of the patient.

Receiver coils can also operate in quadrature. During reception the signals from the two-quadrature modes add constructively, whilst the noise from each is uncorrelated, i.e. it 'averages out', resulting in a $\sqrt{2}$ improvement in SNR over a comparable linear coil.

2.1.9 MRI Artifacts

MRI artifacts are varied and numerous into the physics behind each sequence. Some affect the quality of the MRI exam while others do not affect the diagnostic quality but may be confused with pathology. When encountering an unfamiliar artifact, it is useful to systematically examine general features of the artifact to try and understand the type of artifact and how to negate it if needed (13).These features include:

- Type of sequence (e.g. fast spin echo, or gradient or volumetric acquisition)
- Direction of phase and frequency
- Fat or fluid attenuation
- Presence of anatomy outside the image field
- Presence of metallic foreign bodies

The followings are the example of artifact:

Gibbs artifact is a type of MRI artifacts. It refers to a series of lines in the MR image parallel to abrupt and intense changes in the object at this location, such as the CSF-spinal cord and the skull-brain interface

The MR image is reconstructed from k-space which is a finite sampling of the signal subjected to inverse Fourier transform in order to obtain the final image. At high-contrast boundaries (jump discontinuity in mathematical terms) the Fourier transform corresponds to an infinite number of frequencies, and since sampling is finite the discrepancy appears in the image in the form of a series of lines. These can appear in both phase-encode and frequency-encode direction. The more encoding steps the less intense and narrower the artifacts.

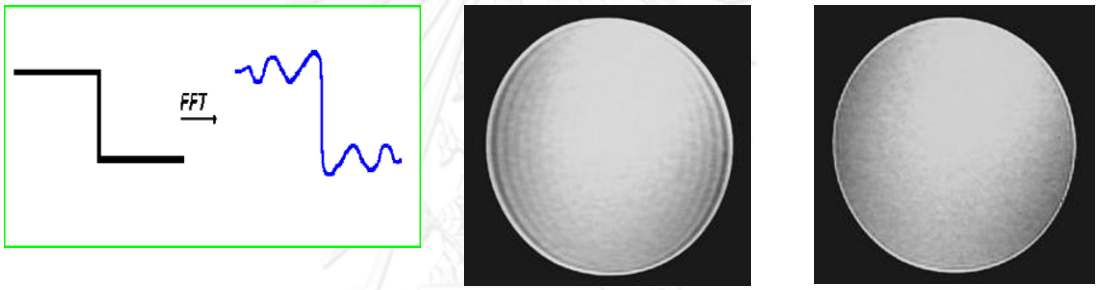

Figure 2.13 Diagram of Gibbs artifact in Fourier transform and in image

(left) the diagram shows the Gibbs effects resulting from Fourier transforming a sharp change in image intensity. Image (middle) shows prominent light and dark line along the sides that fade as they approach the top and bottom of the phantom. Image (right) shows minimal artifact seen uniformly around the periphery of the phantom as a result of increasing the matrix in the phase direction.

Phase-encoded motion artifact is one of many MRI artifacts, and occurs as a result of tissue/fluid moving during the scan and manifests as ghosting in the direction of phase encoding, usually in the direction of short axis of the image (i.e left to right on axial or coronal brains, and anterior to posterior on axial abdomen). These artifacts may be seen from arterial pulsations, swallowing, breathing, peristalsis, and physical movement of a patient. When projected over anatomy it can mimic pathology, and needs to be recognized. Motion that is random such as the patient moving produces a smear in the phase direction. Periodic motion such as respiratory or cardiac/vascular pulsation produces discrete, well defined ghosts. The spacing between these ghosts is related to the TR and frequency of the motion.

Motion artifacts can be distinguished from Gibbs or truncation artifacts because they extend across the entire FOV, unlike truncation artifacts that diminish quickly away from the boundary causing them.

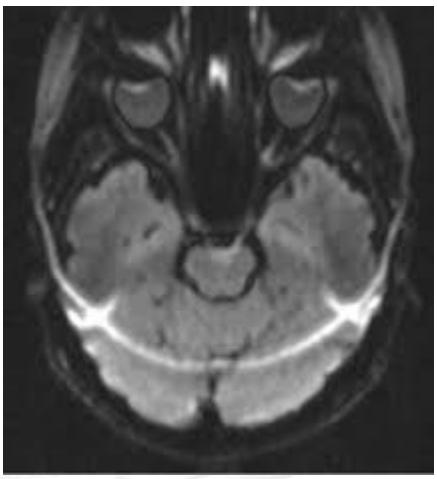

Figure 2.14 EPI image from case of phase encoding artifact in phase direction

Magnetic susceptibility artifact refers to a distortion in the MR image especially seen while imaging metallic orthopedic hardware or dental work. This results from local magnetic field inhomogeneities introduced by the metallic object into the otherwise homogeneous external magnetic field B_0. These local magnetic field inhomogeneities are known as *magnetic susceptibility* and are a property of the object being imaged. In terms of magnetic susceptiblity, most materials can be classified as **diamagnetic, paramagnetic, superparamagnetic, or ferromagnetic.**

Water is considered (weakly) diamagnetic**.**

Paramagnetic materials, which have unpaired electrons, concentrate local magnetic forces and thus increase the local magnetic field, i.e. increase magnetic susceptibility

Superparamagnetic materials contain particles with a much stronger magnetic susceptibility than that of paramagnetic materials. e.g., SPIO (superparamagnetic iron oxide) has been used in liver imaging

Ferromagnetic materials contain large solid or crystalline aggregates of molecules with unpaired electrons exhibit “magnetic memory,” by which a lingering magnetic field is created after their exposure to an external magnetic field. Examples of ferromagnetic metals include iron, nickel, and cobalt, all of which distort magnetic fields, thereby causing severe artifacts on MR images

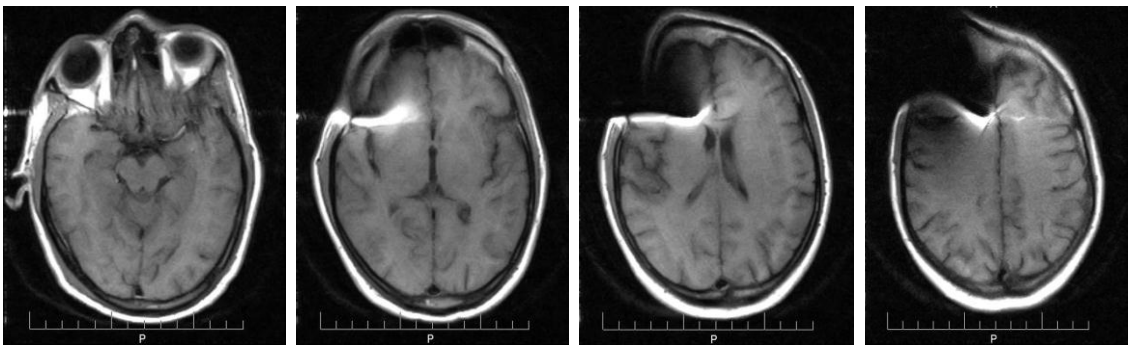

Figure 2.15 MRI image from case of susceptibility artifact cause by metallic material

Aliasing in MRI (also known as wrap-around) is a common MRI artifact that occurs when the field of view (FOV) is smaller than the body-part being imaged. The part of the body that lies beyond the edge of the FOV is projected on to the other side of the image.

This can be corrected, if necessary, by oversampling the data. In the frequency direction, this is accomplished by sampling the signal twice as fast. In the phase direction, the number of phase-encoding steps must be increased with a longer study as a result.

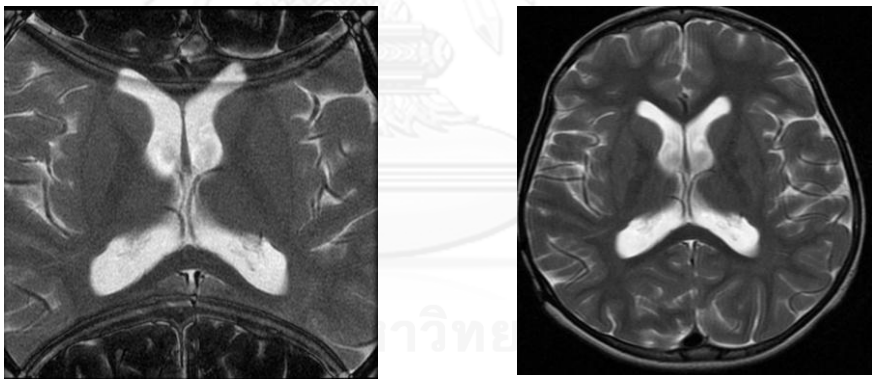

Figure 2.16 Aliasing MRI

Axial T2-weighted images of the brain demonstrate aliasing as in figure 2.16. Right image shows wrap-around with the back of the head projected over the front because the phase-encoded direction is anterior-posterior and the FOV is too small. Left image has the phase and frequency directions reversed resulting in absence of the aliasing artifact. Oversampling was used in the frequency direction to eliminate the aliasing.

2.2 Advances in Magnetic Resonance Imaging

2.2.1 Parallel Imaging (pMRI)

Principles of parallel MRI: Parallel MRI is a recent advance in MRI technology that utilizes simultaneous data acquisitions from multiple RF coil receivers to improve the spatiotemporal resolution of imaging along with reduced k-space sampling schemes forms the core of parallel MRI. The idea of utilizing spatially varying sensitivity from different channels of an RF array to reduce imaging encoding time was initially implemented in different imaging approaches. Currently, there exist two major commercially available implementations of parallel MRI: the image space sensitivity encoding (SENSE) approach, and the k-space spatial harmonics (SMASH) approach, along with its derivative, generalized auto calibrating partial parallel acquisition (GRAPPA). Implementation of parallel MRI requires data from multiple RF coil receivers, each of which observes the spatial distribution of the imaged object's spin density modulated by the coil sensitivity profile of the individual RF coil. The reduced k-space sampling in classical Fourier imaging produces aliased images in individual receivers. Given the coil sensitivity profiles from the RF array, we can unfold these aliased images. Parallel MRI techniques can reduce scan time and thereby improve temporal resolution. Alternatively, parallel MRI can be used to increase the spatial resolution of an image within the same amount of acquisition time. Additional benefits of the parallel MRI technique include lowered susceptibility artifact due to reduced read-out duration, decreased geometrical distortion due to increased phase-encoding bandwidth, and lower echo-planar imaging (EPI) acoustic noise due to reduced gradient switching(4).

Parallel MRI Acquisitions: The purpose of parallel MRI is to avoid "full" sampling of the k-space by skipping certain data collection points. The skipped k-space data produce aliased images, as predicted by the Nyquist sampling theorem. Using information from all channels in the RF coil array, the skipped data can be numerically interpolated from sampled data to restore full field of- view (FOV) images without aliasing artifacts. Parallel MRI skips data in the phase-encoding direction; skipping data in the frequency-encoding direction saves little data acquisition time because the duration of the frequency-encoding gradient is the same regardless of whether sampling is full or skipped. Parallel MRI acquisition with skipped phase encoding data can reduce data acquisition time and thus improve temporal resolution. The benefit of skipping data collection in the phase encoding direction can also be translated to higher bandwidth and less geometrical distortion.

Technical overview of current pMRI methods (14): A brief technical overview over the present pMRI reconstruction methods and strategies is given. To Cartesian-type sampled k-space, in which the number of phase-encoding steps is reduced by the reduction factor R by increasing the distance of equidistantly sampled k-space lines. To maintain resolution, the maximal k-values are left unchanged. In image space, this type of under sampling the k-space yields in a reduced

field of view (FOV) in phase encoding direction associated with fold over artifacts in the coil images as depicted in Figure 2.17

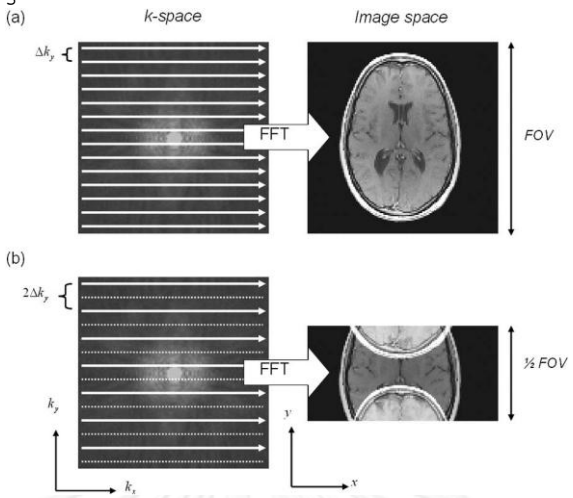

Figure 2.17 pMRI method

(a), Conventional acquisition of fully sampled k-space, resulting in a full FOV image after Fourier transformation. (b), under sampled acquisition (R = 2), resulting in a reduced FOV (FOV/2) with aliasing artifacts. Solid lines indicate acquired k-space lines, dashed lines indicate non acquired k-space lines (14).

Parallel MRI reconstructions (4): Currently, there are two prevailing major variants of reconstruction algorithms: the k-space-based GRAPPA method and the image domain SENSE method. In practice, image reconstruction can be divided into three stages: The first stage is preparation of parallel MRI reconstruction, which includes quantification of array coil performance, coil map estimation, and preprocessing of accelerated data. The second stage is reconstruction of the full-FOV image from under-sampled k-space data. The third stage is combination of reconstructed images for final presentation.

SENSitivity Encoding (SENSE imaging) (14): SENSE is image-base pMRI. It acquisition of reference images give coil sensitivity profiles, speeds up imaging by a factor as much as the maximum number of phase array coil elements. Disadvantage are reduces SNR by at least the same factor as the speed is increased and field of view must be larger than the body part to avoid artifacts.

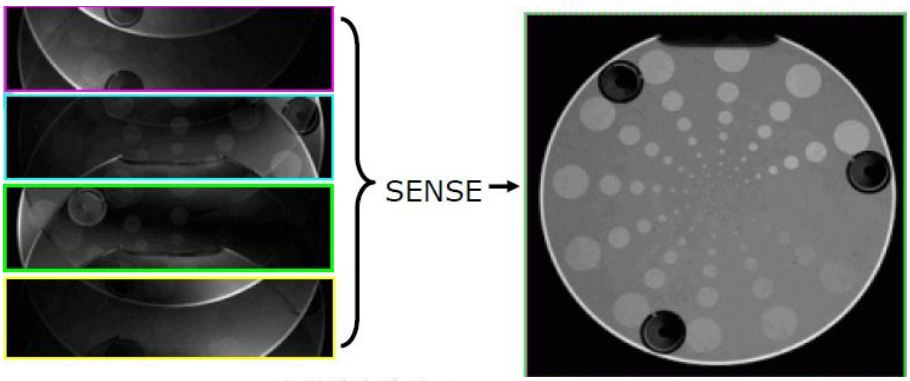

Figure 2.18 Image in SENSE reconstruction

Data acquired from each PA coil element goes into reconstruction of whole image – reduces imaging time, reduces SNR, reduces uniformity(14).

GeneRalized Auto calibrating Partially Parallel Acquisitions (GRAPPA) (14): GRAPPA came from Auto-calibration methods. The basic of auto-calibration are missing k-space lines which are synthesized using linear least squares fitting between reference data and nearest neighbor lines of data. It is fitting determines the weighting factors for generating missing lines for each coil. The fouriertranform is then used to produce uncombined image for each coil. GRAPPA is k-space based pMRI, k-space based approach assumes spatial harmonics of phase-encoding gradients can be omitted and emulated by a linear combination of coil sensitivities, it acquires reference lines (ACS lines) in k-space rather than whole coil sensitivity images and the acceleration achieved by omitting phase-encoding steps during acquisition and reconstructing missing data from the redundant information in the signals captured by different array elements.

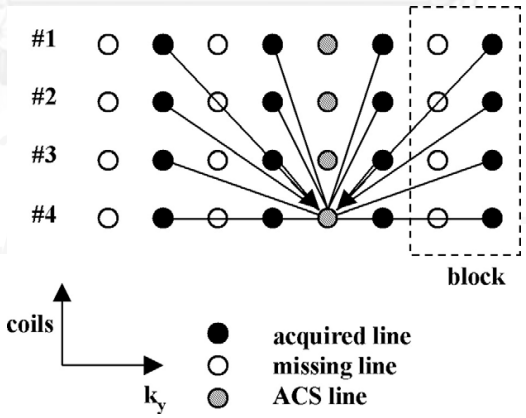

Figure 2.19 Scheme of the GRAPPA approach.

Multiple lines acquired for the different coils are fitted to the auto calibration signal (ACS) data. Here, four lines are employed to fit a single ACS line in coil 4. The dotted line area indicates a block used in the GRAPPA approach.

2.2.2 Advance technique in MRI

Fast Spin Echo (FSE) (5): Fast spin echo (FSE), also known as turbo spin echo (TSE) is a commercial version of RARE (Rapid Acquisition with Relaxation Enhancement) with evenly spaced multiple refocusing pulses(commonly but not always,180^{o}) forming an echo train. These extra echoes are not used to acquire free images with different TE but are used to acquire multiple lines of data, i.e. to have *different* phase encoding for *each* echo. The Inter Echo Spacing (IES or ESP, echo spacing) is the time between successive echoes. This is always a fixed value as the RF pulses are all evenly spaced apart in time to avoid problems with *coherence pathways*. The echo train length (ETL) or turbo factor (TF) is the number of echoes in the spin echo train. In FSE lines of k-space are acquired from different echoes the *effective echo time* (TE_{eff}) is the echo time that dominates the image contrast.

Echo Planar Imaging (EPI) (15): Basic concepts to fully understand echo-planar imaging, one must be familiar with the concepts of gradient spatial encoding, k space, and k-space mapping

k-space: k-space is a coordinate system used to organize the gradient-derived spatial frequency information prior to the inverse Fourier transform and final image reconstruction(figure 2.18). Low spatial frequencies (large objects and image contrast) are encoded in the center of k-space, and high spatial frequencies (small objects and fine detail) are encoded at the periphery. K space is not a grid that can be directly overlaid on the image. Each point in k-space represents a spatial frequency over the entire image. The range of spatial frequencies in k-pace can also be thought of as coding for different degrees of edge definition. Collecting data only in the center of k space produces a low-resolution, blurry image with unsharp edges, whereas adding data into the periphery produces a high-resolution image with sharp edge detail. Other important properties of this scheme are that points in the center of k space, which are collected at the peak intensity of the signal echo, dominate image contrast and the signal-to-noise ratio (S/N) but are sensitive to motion artifacts. Conversely, points at the periphery of k-space, which are collected from less intense segments of the echo, have less effete on image contrast but determine maximum spatial resolution and noise in the image and produce fewer from motion.

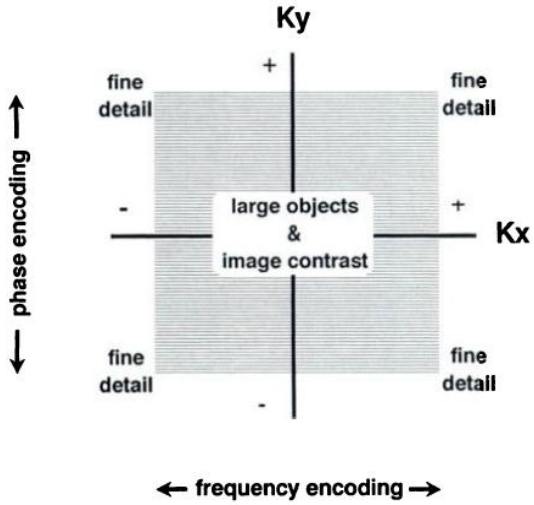

Figure 2.20 Diagram of k-space

k-space Mapping: (15) The simplest conventional method of k-space mapping is the application of gradients that encode all points across the frequency (x) direction with each pulse cycle whereas the phase (y) direction is encoded in single steps during successive cycles, separated by the TR interval. This accounts for the relatively long imaging times of conventional MR imaging. Faster imaging has been achieved on conventional images by using rapid acquisition with relaxation enhancement (RARE) or fast SE (FSE) techniques that map multiple phase-encoding steps with each pulse cycle.

EPI Features (15): The key feature of echo-planar imaging that allows fast imaging is the use of rapid gradient switching to acquire all frequency-encoding points and all phase-encoding steps during a single pulse cycle (figure 2.21). Evolution of this technique improved k-space coverage and replaced the constant phase-encoding gradient with short gradient- pulse “blibs,” resulting in the modulus- blipped echo-planar single-pulse technique (MBEST)

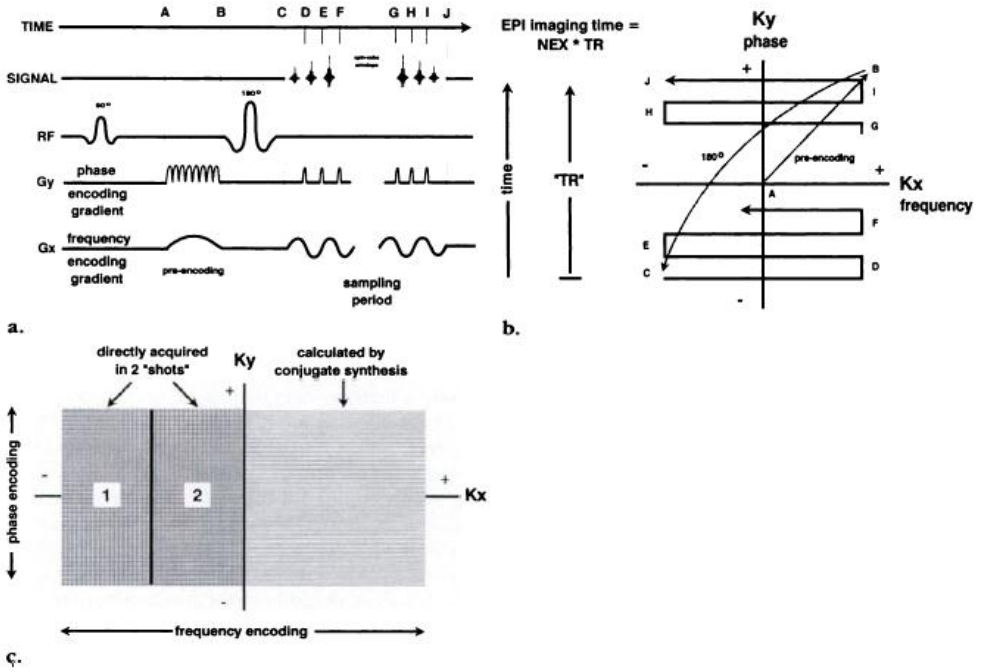

Figure 2.21 (a) Diagram of Echo planar imaging, (b) Diagram of echo planar k-space mapping and (c) Diagram of mosaic partial k-space mapping.

(a) Diagram of an echo-planar imaging SE pulse sequence shows echo-planar spatial encoding. A pre-encoding pulse is applied to both gradients between the RF pulses and prior to the MR signal sampling period (A to B). Rapid gradient switching is used to acquire all phase and frequency spatial-encoding points during one sampling period (C through]). This is done by oscillating the frequency-encoding gradient in a sinusoidal fashion and “blipping” the phase-encoding gradient at the zero-crossing points of the frequency-encoding gradient. Gradient echoes are generated within the SE envelope at the center of each lobe of the oscillating frequency-encoding gradient. Single-”shot” (single-acquisition) image data collection is reduced to the duration of the SE sampling period (as short as 20 msec). (b) Diagram of echo-planar k-space mapping shows the k-space trajectory traced by the echo-planar imaging (EPI) SE pulse sequence. Positive pre-encoding pulses are applied after the 90° RF excitation and displace the spatial frequency encoding an equal amount in each axis (A to B). The subsequent 180° inversion pulse flips the spatial-encoding point to the opposite corner of k space (B to C). Initial application of the frequency-encoding gradient alone causes horizontal displacement along the Kx axis (C to D). The positive pulse of the phase-encoding gradient at this point (D) step up the trajectory, and the subsequent negative lobe of the oscillating frequency-encoding gradient generate a horizontal line in the opposite direction (D to E). This sequence is repeated throughout the sampling period (C through]) at the 1-kHz oscillation rate of the frequency-encoding gradient (500 psec between each phase-encoding step). The result is a symmetric rectilinear trajectory through k space. Because there is no repetition of a single-shot image, the TR interval is infinite and is shown as open-ended in the figure. Multiple shots or multiple excitations (NEX) are separated by TR

intervals. (c) Diagram of “mosaic” partial k-space mapping shows a “partial-read mosaic” scheme in which only part of k space is directly acquired (in two shots). Because k space is symmetrically redundant, these data can be “tiled” in a mosaic along the frequency-encoding or read axis and the rest of k space can be mathematically generated by means of conjugate synthesis (15).

S**ingle-shot echo-planar images**, there is no repetition of the pulse cycle, so that the TR can be thought of as open-ended or infinite. This affects tissue contrast by eliminating the T1 partial saturation usually produced by repeating the pulse cycle in conventional sequences and so provides images that are truly T2 weighted. These infinite and long TR pulse sequences allow direct acquisition of T2-weighted GRE and SE images but not of Ti-weighted SE images.

The sensitivity of echo-planar imaging to magnetic susceptibility differences occurs for similar reasons. Like chemical shifts, magnetic susceptibility gradients between structures cause frequency shifts, which result in artifactual signal displacement and local image distortion. This effect is combined with signal loss caused by susceptibility gradient T2* shortening and appears most prominently at air-bone-tissue interfaces such as those at the paranasal sinuses, orbits, and petrous ridges in the head.

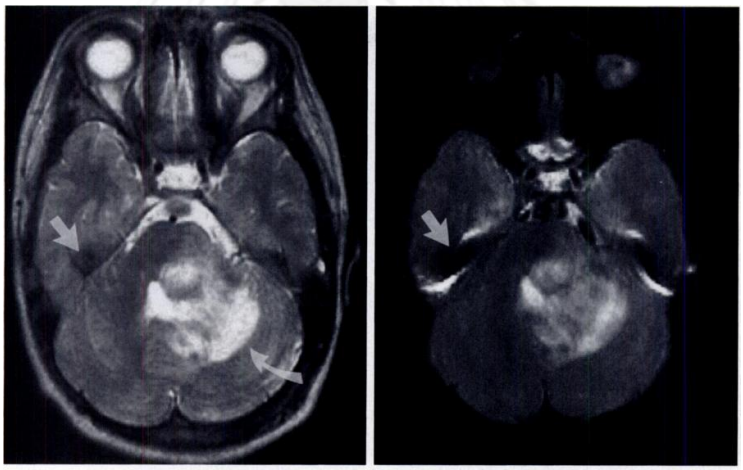

Figure 2.22 Skull base magnetic susceptibility artifact.

(a) FSE T2-weighted image shows high signal intensity in a pontocenebellar neoplasm (curved arrow). Low signal intensity is seen at the apex of the petrous bone (straight arrow). (b) Echo-planar T2-weighted image shows the high-signal-intensity pontocerebellar lesion well but also shows more prominent magnetic susceptibility artifact at the ridges of the petrous bone (arrow). (15)

Parallel Imaging reduces susceptibility artifacts: With parallel imaging, the time needed to traverse the k-space is reduced by means of mathematically “unfolding” the aliased images from individual receivers in the array. Reduced k-space traversing time also benefits the reduction of susceptibility artifacts and geometrical distortion originating from local magnetic field

inhomogeneity. This is because the shortened readout time for data acquisition contributes to reduced local spin dephasing within individual voxels and produces higher bandwidth in the phase-encoding direction (4)

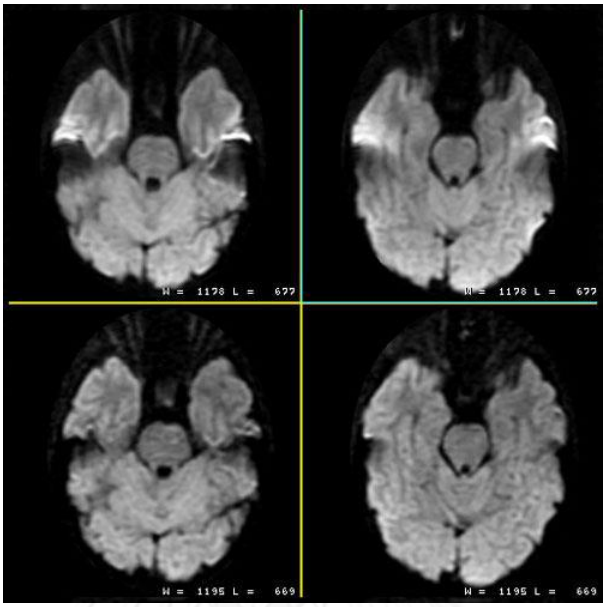

Figure 2.23 (Top) Single Shot EPI in normal acquisition, (bottom) Single Shot EPI with parallel image (acceleration factor =2) (16)

2.3 Review of Related Literature

F.-H. Lin and S.-Y. Tsai. Parallel Magnetic Resonance Imaging Acquisition and Reconstruction: Application to Functional and Spectroscopic Imaging in Human Brain: Method of Cancer, Therapy and Prognosis Volume 8(2011):245-262 (4).Demonstrate the effect of reduced Echo Planar Imaging (EPI) distortion with GRAPPA in case Functional MRI on 3T scanner (Siemens Medical Solution, Erlangen, Germany) equipped with an eight-channel head phased array Coil. The imaging parameters are: FOV equals 200 mm, TR/TE equals 2,000/30 ms, Flip angle equals 90°, slice thickness equals 3 mm, bandwidth equals 1,440 Hz. Phase encoding was in the anteroposterior direction.

The result showed image distortion around the frontal and temporal lobes was improved using GRAPPA imaging. Regularization can also suppress noise at the center of the reconstructed image, compared to un-regularized reconstruction in the same acceleration rate.

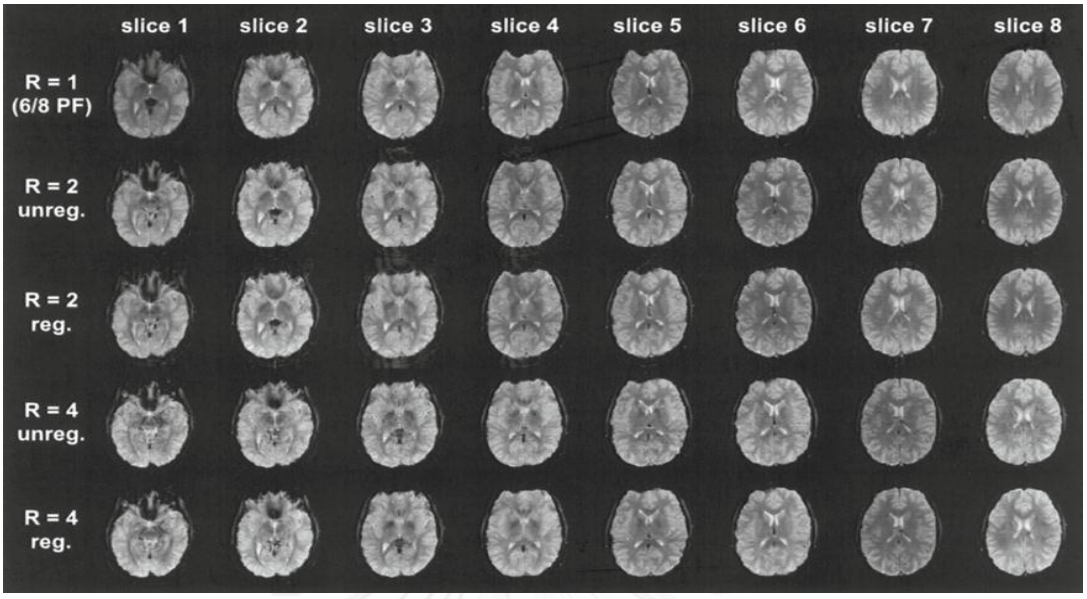

Figure 2. 24 Comparison of non-acceleration factor (R=1) with GRAPPA acceleration factor at 2 and 4

Compare non-accelerated reconstruction (R = 1) with 6/8 partial Fourier (PF) sampling, GRAPPA EPI reconstructions at 2X (R = 2) and 4X (R = 4) accelerations show decreased distortion around the temporal and frontal lobes, where susceptibility and B_0 inhomogeneity is strong. At the same acceleration rate, regularized (reg.) reconstructions show less noise amplification than unregularized (unreg.) reconstructions, particularly around the center of the brain.

Blaimer M.Breuer F., Mueller M., Heidemann R.M., Griswold M.A., and Jakob P.M. SMASH, SENSE, PILS, GRAPPA How to Choose the Optimal Method. Top Magn Reson Imaging. 15(2004): 223–236 (14). A Comparison: SENSE Versus GRAPPA. Because of their availability for daily clinical routine, the following section addresses advantages and disadvantages of both SENSE and GRAPPA. Although both methods are different approaches to reconstruct missing data, they provide very good results with nearly identical reconstruction quality and are therefore well suited to enhance almost every clinical application.

However, image reconstruction of single-shot EPI applications with SENSE is problematic because the distortions in EPI images and coil sensitivity maps are different. This means that the image intensity at a given location may not correspond to the correct value in the sensitivity map. Possible solutions have been reported to overcome this problem with SENSE. GRAPPA has proven to be well suited for EPI, since the k-space based reconstruction of missing lines is not affected by image distortions. In almost every area tested so far, GRAPPA showed robust

reconstructions without modifying either the EPI sequence or the reconstruction algorithm as shown in figure 2.25

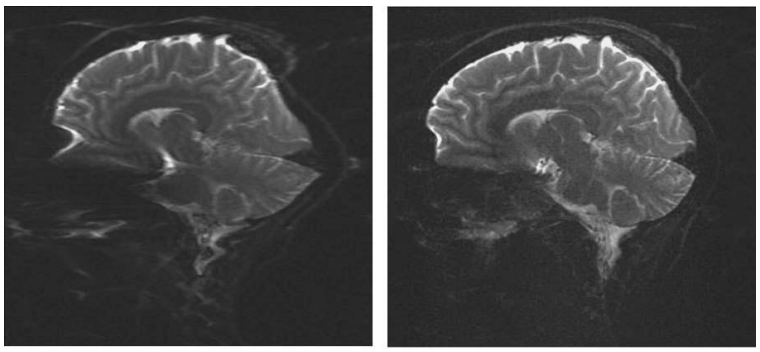

Figure2. 25 Reduced distortions in Single-Shot Echo-Planar Imaging (EPI) by the use of pMRI, acquired with an eight-element head coil array.

(a) Conventional EPI with 128 x 256 matrix size. (b) With GRAPPA using an acceleration factor of 3, the resolution is doubled to 256 x 256. Furthermore, this image shows reduced distortions.

Y.A. Bhagat, D.J. Emery, S. Naik, T. Yeo, C. Beaulieu. Comparison of Generalized Autocalibrating Partially Parallel Acquisitions and Modified Sensitivity Encoding for Diffusion Tensor Imaging. AJNR Am J Neuroradiol 28(2007):293–98 **(17)**. To evaluate which parallel imaging can lessen these artifacts by shortening the length of the echo-train acquisition. The self-calibrating parallel acquisition techniques, image domain-based modified sensitivity encoding (mSENSE) and *k*-space-based generalized auto calibrating partially parallel acquisitions (GRAPPA), with DTI of brain in 5 healthy subjects. The results showed that the reviewers scored the GRAPPA and mSENSE R = 2 images better than images acquired with conventional techniques. FA contrast was improved at the GM/WM junction in peripheral brain areas. Trace/3 ADC and FA measurements were consistent for all methods. However, R = 3 and 4 images suffered from reconstruction-related artifacts.

CHAPTER III

RESEARCH METHODOLOGY

3.1 Research Design

This study is an experimental research.

3.2 Research Design Model

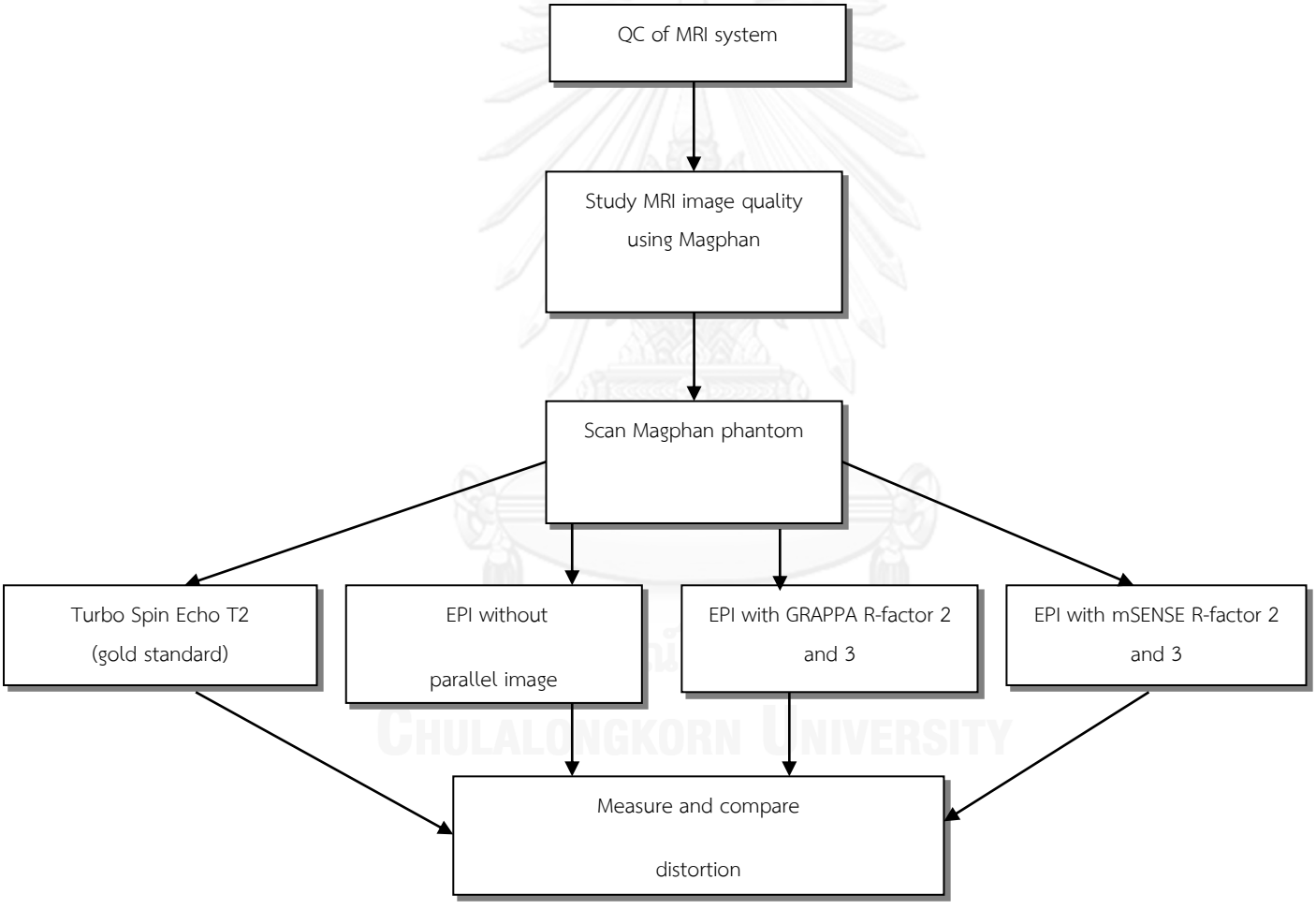

Figure 3.1 Research design model

3.3 Conceptual Framework

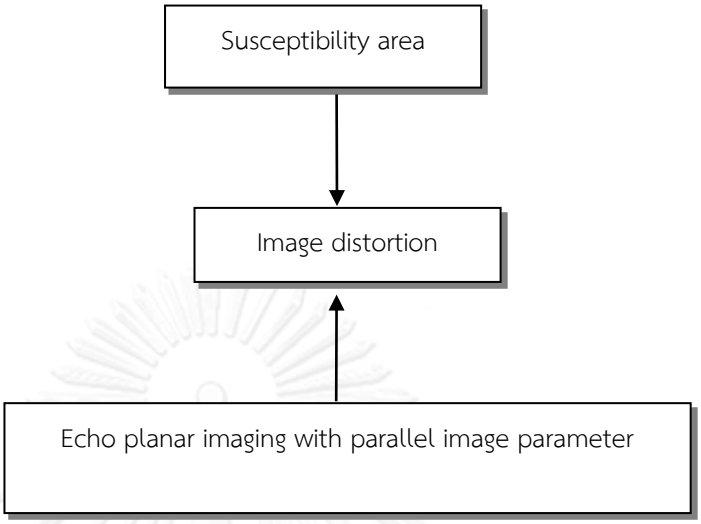

Figure 3.2 Conceptual framework

3.4 Research Question

Which parameter (GRAPPA and mSENSE) reduces distortion diffusion weighted imaging in Echo Planar Imaging?

3.5 Materials

3.5.1 MRI 1.5 Tesla, Siemens Medical System: Magnetom, Aera

MRI 1.5 Tesla, with 70 cm magnet bore, digital coil and auto calibration software version D13, was installed at King Chulalongkorn Memorial Hospital in 2012.

Figure 3.3 MRI 1.5 Tesla (Siemens Medical System: Magnetom, Germany)

3.5.2 12-element phase array head coil

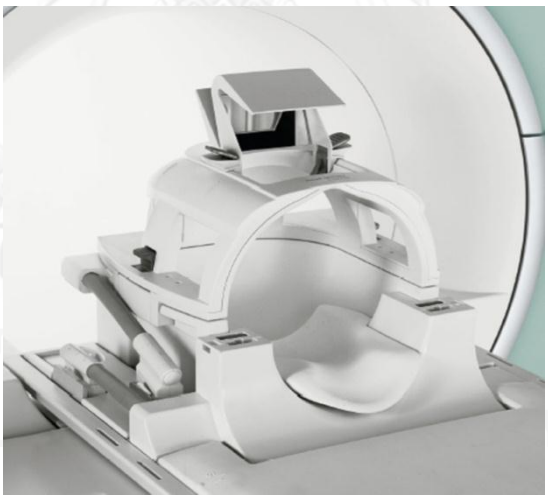

Figure 3.4 12-Element Phase array head coil

The 12 element is dome design which consists of two rings of 6 elements each. It produces exceptional signal-to-noise ratio improvements at 1.5T. Uniformity and design for smoothly integrated into the head imaging or high performance coil for brain procedures.

3.5.3 MRI MAGPHAN PHANTOM

Figure 3. 5 MRI Magphan phantom

The Magphan phantom model SMR170: the urethane cylinder has an outer diameter of 200 mm and inner diameter of 190 mm. The phantom was filled with $CuSO_4$ solution at only half of phantom, in order to represent the susceptibility area.

3.5.4 Image J Program

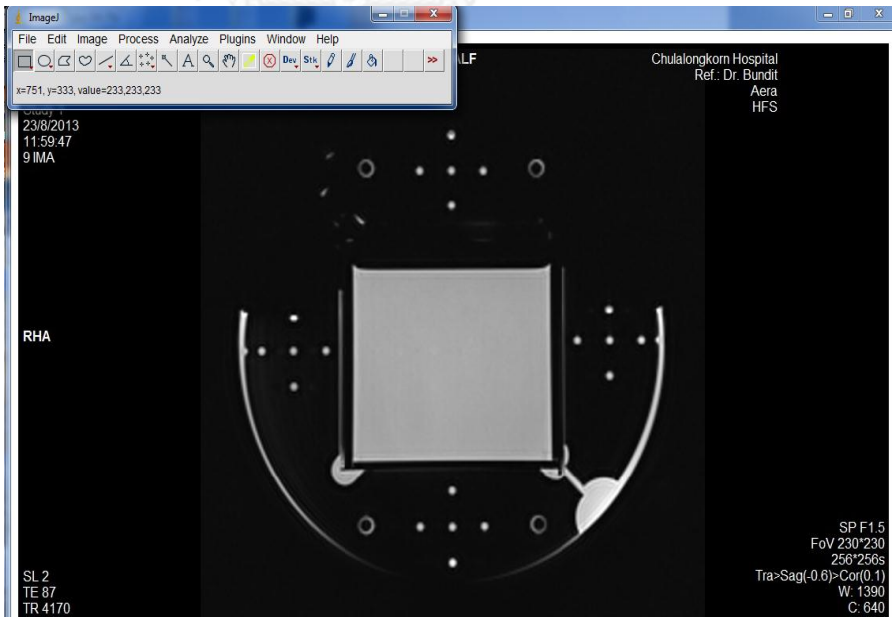

Figure 3.6 Image J program

Image J is a program installed and run on Windows. The co-ordinate can be measured using this program.

3.6 Methods

3.6.1 QC for MRI scanner

The quality control of MRI 1.5 Tesla was performed following ACR manual (2004). The QC procedures were:

3.6.1.1 High contrast resolution

3.6.1.2 Low contrast detectability

3.6.1.3 Slice thickness accuracy

3.6.1.4 Slice position accuracy

3.6.1.5 Geometric distortion

3.6.1.6 Image uniformity

3.6.1.7 Percent signal ghosting

3.6.2 Magphan phantom scan

The pulse sequence acquisition parameters as shown in Table 3.1 were set for Magphan phantom scan.

Table 3.1 Pulse sequence acquisition parameters

Pulse sequence	TR (msec)	TE (msec)	FOV (mm)	Slice thickness (mm)	Slice gap (mm)	Matrix	Bandwidth
TSE T2	5500	171	230x230	2	0	256x256	Variable
EPI without parallel image	5500	171	230x230	2	0	200x200	Variable
EPI with mSENSE 2	4300	171	230x230	2	0	200x200	Variable
EPI with mSENSE 3	3900	171	230x230	2	0	200x200	Variable
EPI with GRAPPA 2	4300	171	230x230	2	0	200x200	Variable
EPI with GRAPPA 3	3900	171	230x230	2	0	200x200	Variable

TR: Repetition time, TE: Echo time, TSE: Turbo spin echo, FOV: Field of view, Matrix: matrix size.

3.6.3 Record the co-ordinate of each object from 3 locations in Magphan.

Using image J program to determine the co-ordinate(x,y) of 5 objects from 3 locations in pulse sequence acquisition parameter: Turbo Spin Echo(TSE) T2, Echo Planar Imaging(EPI) without parallel image, EPI with parallel image (GRAPPA and mSENSE) in EPI technique, b-value, b0 and b1000.

3.7 Sample size determination

The sample size was calculated for number of scan as following.

TSE T2 = 3

EPI without parallel image = 3

EPI with GRAPPA R-factor 2 = 3

EPI with GRAPPA R-factor 3 = 3

EPI with mSENSE R-factor 2 = 3

EPI with mSENSE R-factor 3 = 3

Total = 18

3.8 Statistical analysis

The Image J was used to determine co-ordinate and evaluate the distortion. Percent deviation was calculated by equation.

$$\text{Percent deviation} = [(\text{variable parameters} - \text{TSE T2})/\text{TSE T2}] \times 100$$

3.9 Outcome measurement

Phantom study

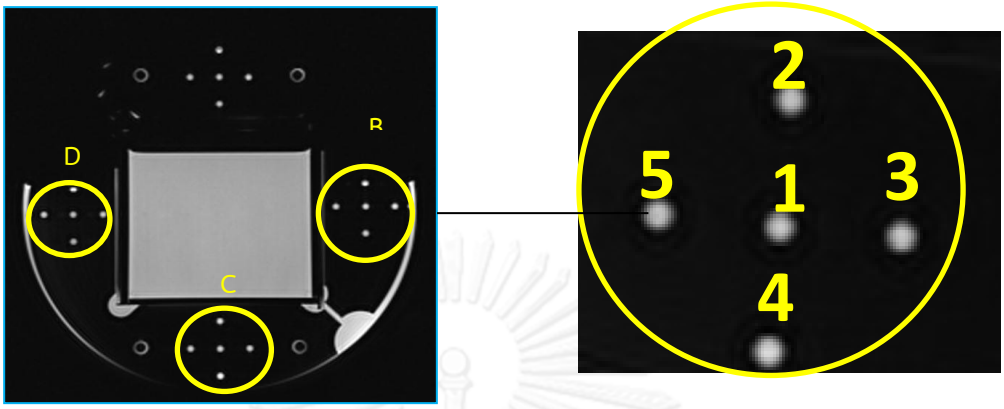

Figure 3.7 Left: locations of group of 5 objects B, C, D, Right : position of each location of 5 objects.

Record co-ordinate(x,y) in each group at 3 o'clock (B), 6 o'clock (C),and 9 o'clock (D), of 5 objects of each group.

Independent variables: Parameter in EPI with and without parallel image, Time repetition (TR), Variable Bandwidth, Matrix size.

Dependent variables: Slice thickness, Slice gap, Time to Echo (TE), Field of view (FOV).

3.10 Expected benefit

The parameters used to reduce distortion artifact at susceptibility area, when scan technique Diffusion weighted Imaging (DWI) at MRI 1.5 Tesla.

3.11 Ethical consideration

Although this study is performed in phantom only, the ethic had been approved by the Ethics Committee, Faculty of Medicine Chulalongkorn University.

CHAPTER IV

RESULTS

4.1 Quality control of MRI scanners

The quality control of 1.5 Tesla MRI system was performed by following the ACR manual (2008). The results of image uniformity, high contrast resolution, low contrast detectability, slice thickness accuracy, slice position accuracy and geometric distortion are shown in Appendix B. The report of MRI system performance test is shown in Table 4.1

Table 4.1 REPORT OF MRI 1.5T PERFORMANCE TEST

LOCATION	King Chulalongkorn Memorial Hospital
DATE	JUNE 7,2013
MANUFACTURER	Siemens
MODEL	Magnetom, Aera 1.5 Tesla
SOFTWARE VERSION	D13
Image Intensity Uniformity	Pass
Percent-Signal Ghosting	Pass
Low Contrast Detectability	Pass
Slice Thickness Accuracy	Pass
Slice Position Accuracy	Pass
Geometric Distortion	Pass
High Contrast Resolution	Pass

4.2 Pulse sequence acquisition parameters data

The pulse sequences are Turbo Spin Echo T2 (gold standard) , Echo Planar Imaging (EPI) without parallel Image, Echo Planar Imaging (EPI) with parallel image which consist of mSENSE R-factor 2, Echo, mSENSE R-factor 3, GRAPPA R-factor 2, GRAPPA R-factor3 in scan parameter without parallel image and with parallel image record in b-value: b0 and b 1000. The table of pulse sequence is shown in Table 4.2

Table 4.2 Pulse sequence parameters

Pulse sequence	TR (msec)	TE (msec)	FOV (mm)	Slice thickness (mm)	Slice gap (mm)	Matrix	Scan time
TSE T2	5500	171	230x230	2	0	256x256	2 min 30 sec
EPI without parallel image	5500	171	230x230	2	0	200x200	2min 20sec
EPI with mSENSE 2	4300	171	230x230	2	0	200x200	1min 32sec
EPI with mSENSE 3	3900	171	230x230	2	0	200x200	1min 31sec
EPI with GRAPPA 2	4300	171	230x230	2	0	200x200	1min 32 sec
EPI with GRAPPA 3	3900	171	230x230	2	0	200x200	1min 31sec

4.3 The co-ordinate of variation parameters at each location

Record the co-ordinate of variation parameters at each location, 5 objects per each by using image J program as shown in Table 4.3- 4.13. Object position is shown in figure 4.1.

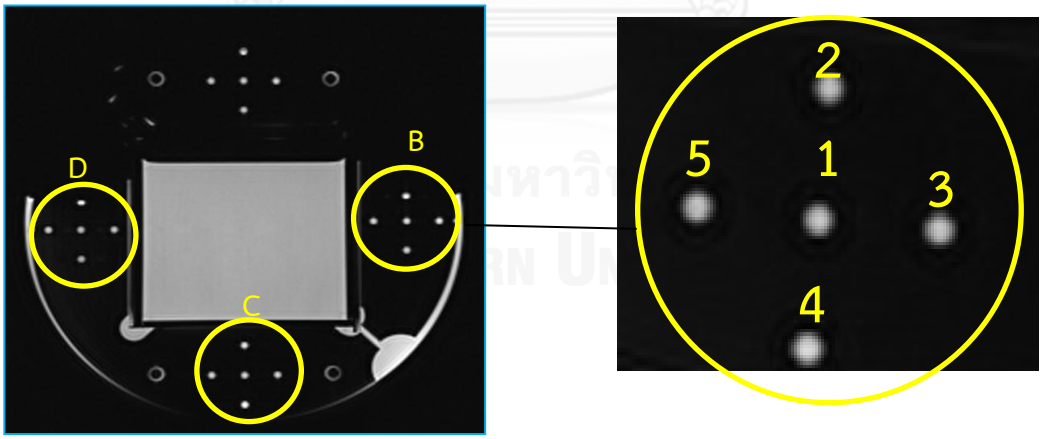

Figure 4.1 (left) 3 locations (B, C, D), (right) position of 5 objects per each location

Magphan phantom image in variation parameters were shown in figure 4.2

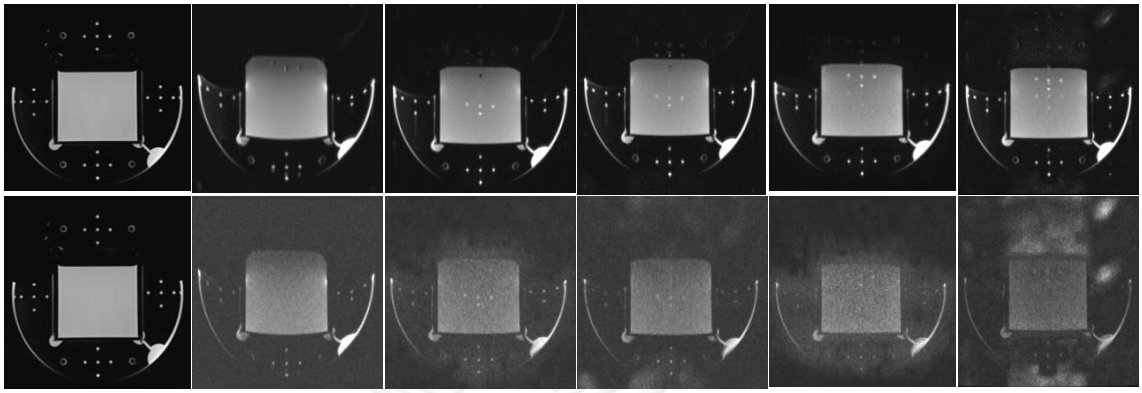

Figure 4. 2 Magphan phantom scan image

Upper row images are in b 0 and lower row are in b 1000; (left to right) TSE T2 , EPI without parallel image, EPI with GRAPPA R-factor 2, EPI with mSENSE R-factor 2, EPI with GRAPPA R-factor 3, EPI with mSENSE R-factor 3

Table 4.3 Co-ordinate (x,y) at each location of scan parameter TSE T2

Location B										
Object number	1		2		3		4		5	
Co-ordinate	x	y	x	y	x	y	x	y	x	y
Co-ordinate point	750	333	750	300	790	333	750	373	710	333

Location C										
Object number	1		2		3		4		5	
Co-ordinate	x	y	x	y	x	y	x	y	x	y
Co-ordinate point	551	544	550	502	592	543	551	584	510	544

Location D										
Object number	1		2		3		4		5	
Co-ordinate	x	y	x	y	x	y	x	y	x	y
Co-ordinate point	348	345	348	308	389	349	349	385	308	345

Table 4.4 Co-ordinate(x,y) at each location of scan parameter EPI without parallel image at b0.

Location B										
Object number	1		2		3		4		5	
Co-ordinate	x	y	x	y	x	y	x	y	x	y
Co-ordinate point	751	345	n/a	n/a	791	325	751	365	710	348

Location C										
Object number	1		2		3		4		5	
Co-ordinate	x	y	x	y	x	y	x	y	x	y
Co-ordinate point	551	556	550	516	592	554	552	589	509	555

Location D										
Object number	1		2		3		4		5	
Co-ordinate	x	y	x	y	x	y	x	y	x	y
Co-ordinate point	348	337	n/a	n/a	389	346	349	369	308	320

Table 4.5 Co-ordinate(x,y) at each location of scan parameter EPI without parallel image at b1000.

Location B										
Object number	1		2		3		4		5	
Co-ordinate	x	y	x	y	x	y	x	y	x	y
Co-ordinate point	751	344	n/a	n/a	791	326	751	365	710	348

Location C										
Object number	1		2		3		4		5	
Co-ordinate	x	y	x	y	x	y	x	y	x	y
Co-ordinate point	550	556	550	516	592	554	550	590	509	556

Location D										
Object number	1		2		3		4		5	
Co-ordinate	x	y	x	y	x	y	x	y	x	y
Co-ordinate point	348	337	n/a	n/a	389	346	349	369	309	321

Table 4.6 Co-ordinate(x,y) at each location of scan parameter EPI with GRAPPA R-factor 2 at b0.

Location B										
Object number	1		2		3		4		5	
Co-ordinate	x	y	x	y	x	y	x	y	x	y
Co-ordinate point	751	337	n/a	n/a	790	329	751	367	710	339

Location C										
Object number	1		2		3		4		5	
Co-ordinate	x	y	x	y	x	y	x	y	x	y
Co-ordinate point	550	549	551	507	592	548	551	586	510	548

Location D										
Object number	1		2		3		4		5	
Co-ordinate	x	y	x	y	x	y	x	y	x	y
Co-ordinate point	349	340	n/a	n/a	389	344	349	376	309	331

Table 4.7 Co-ordinate(x,y) at each location of scan parameter EPI with GRAPPA R-factor 2 at b1000.

Location B										
Object number	1		2		3		4		5	
Co-ordinate	x	y	x	y	x	y	x	y	x	y
Co-ordinate point	751	337	n/a	n/a	790	329	750	369	709	340

Location C										
Object number	1		2		3		4		5	
Co-ordinate	x	y	x	y	x	y	x	y	x	y
Co-ordinate point	550	549	550	508	591	548	551	585	510	548

Location D										
Object number	1		2		3		4		5	
Co-ordinate	x	y	x	y	x	y	x	y	x	y
Co-ordinate point	349	340	n/a	n/a	389	345	348	377	308	331

Table 4.8 Co-ordinate(x,y) at each location of scan parameter EPI with GRAPPA R-factor 3 at b0.

Location B										
Object number	1		2		3		4		5	
Co-ordinate	x	y	x	y	x	y	x	y	x	y
Co-ordinate point	751	335	n/a	n/a	790	329	750	369	709	337

Location C										
Object number	1		2		3		4		5	
Co-ordinate	x	y	x	y	x	y	x	y	x	y
Co-ordinate point	551	547	550	506	592	545	550	584	510	545

Location D										
Object number	1		2		3		4		5	
Co-ordinate	x	y	x	y	x	y	x	y	x	y
Co-ordinate point	348	340	n/a	n/a	389	344	349	378	308	335

Table 4.9 Co-ordinate(x,y) at each location of scan parameter EPI with GRAPPA R-factor 3 at b1000.

Location B										
Object number	1		2		3		4		5	
Co-ordinate	x	y	x	y	x	y	x	y	x	y
Co-ordinate point	750	337	n/a	n/a	791	330	750	370	708	338

Location C										
Object number	1		2		3		4		5	
Co-ordinate	x	y	x	y	x	y	x	y	x	y
Co-ordinate point	549	545	550	505	591	545	551	583	510	544

Location D										
Object number	1		2		3		4		5	
Co-ordinate	x	y	x	y	x	y	x	y	x	y
Co-ordinate point	348	342	n/a	n/a	389	345	349	379	306	336

Table 4.10 Co-ordinate(x,y) at each location of scan parameter EPI with mSENSE R-factor 2 at b0.

Location B										
Object number	1		2		3		4		5	
Co-ordinate	x	y	x	y	x	y	x	y	x	y
Co-ordinate point	750	336	n/a	n/a	791	326	751	366	710	337

Location C										
Object number	1		2		3		4		5	
Co-ordinate	x	y	x	y	x	y	x	y	x	y
Co-ordinate point	550	547	550	506	592	546	550	583	510	546
Location D										
Object number	1		2		3		4		5	
Co-ordinate	x	y	x	y	x	y	x	y	x	y
Co-ordinate point	349	338	n/a	n/a	390	342	349	375	308	329

Table 4.11 Co-ordinate(x,y) at each location of scan parameter EPI with mSENSE R-factor 2 at b1000.

Location B										
Object number	1		2		3		4		5	
Co-ordinate	x	y	x	y	x	y	x	y	x	y
Co-ordinate point	751	334	n/a	n/a	791	324	751	363	709	336

Location C										
Object number	1		2		3		4		5	
Co-ordinate	x	y	x	y	x	y	x	y	x	y
Co-ordinate point	551	549	551	507	592	546	550	585	510	548

Location D										
Object number	1		2		3		4		5	
Co-ordinate	x	y	x	y	x	y	x	y	x	y
Co-ordinate point	348	337	n/a	n/a	391	343	349	374	308	328

Table 4.12 Co-ordinate(x,y) at each location of scan parameter EPI with mSENSE R-factor 3 at b0.

Location B										
Object number	1		2		3		4		5	
Co-ordinate	x	y	x	y	x	y	x	y	x	y
Co-ordinate point	751	333	n/a	n/a	790	327	750	367	710	335

Location C										
Object number	1		2		3		4		5	
Co-ordinate	x	y	x	y	x	y	x	y	x	y
Co-ordinate point	551	544	551	503	592	543	552	583	510	544

Location D										
Object number	1		2		3		4		5	
Co-ordinate	x	y	x	y	x	y	x	y	x	y
Co-ordinate point	349	340	n/a	n/a	389	342	349	377	309	333

Table 4.13 Co-ordinate(x,y) at each location of scan parameter EPI with mSENSE R-factor 3 at b1000.

Location B										
Object number	1		2		3		4		5	
Co-ordinate	x	y	x	y	x	y	x	y	x	y
Co-ordinate point	n/a	n/a	n/a	n/a	792	328	n/a	n/a	n/a	n/a

Location C										
Object number	1		2		3		4		5	
Co-ordinate	x	y	x	y	x	y	x	y	x	y
Co-ordinate point	551	549	550	507	591	548	551	585	509	548

Location D										
Object number	1		2		3		4		5	
Co-ordinate	x	y	x	y	x	y	x	y	x	y
Co-ordinate point	n/a	n/a	n/a	n/a	n/a	n/a	n/a	n/a	n/a	n/a

4.4 Deviation of co-ordinate in each sequence

The deviation of co-ordinate in each of pulse sequence was calculated by

(Co-ordinate of variation sequence) – (Co-ordinate of TSE T2)

Note: The deviation value show in plus (+) and minus (-) these sign represent the distortion direction in plus (+) as up and minus (-) as down directions.

Table 4.14 Deviation at each co-ordinate compare with sequence TSE T2 in b0 at location B

Deviation at each co-ordinate compared with sequence TSE T2 in b0					
Co-ordinate	EPI without parallel image	EPI with GRAPPA R-factor 2	EPI with mSENSE R-factor 2	EPI with GRAPPA R-factor 3	EPI with mSENSE R-factor 3
x1	-1	-1	0	-1	-1
y1	-12	-4	-3	-2	0
x2	n/a	n/a	n/a	n/a	n/a
y2	n/a	n/a	n/a	n/a	n/a
x3	-1	0	-1	0	0
y3	8	4	7	4	6
x4	-1	-1	-1	0	0
y4	8	6	7	4	6
x5	0	0	0	1	0
y5	-15	-6	-4	-4	-2

Table 4.15 Deviation at each co-ordinate compare with sequence TSE T2 in b1000 at location B

Deviation at each co-ordinate compared with sequence TSE T2 in b0					
Co-ordinate	EPI without parallel image	EPI with GRAPPA R-factor 2	EPI with mSENSE R-factor 2	EPI with GRAPPA R-factor 3	EPI with mSENSE R-factor 3
x1	-1	-1	-1	0	n/a
y1	-11	-4	-1	-4	n/a
x2	n/a	n/a	n/a	n/a	n/a
y2	n/a	n/a	n/a	n/a	n/a
x3	-1	0	-1	0	-0.25
y3	7	4	9	2	1.5
x4	-1	0	-1	0	n/a
y4	8	4	10	3	n/a
x5	0	1	1	2	n/a
y5	-15	-7	-3	-5	n/a

Table 4.16 Deviation at each co-ordinate compare with sequence TSE T2 in b0 at location C

Deviation at each co-ordinate compared with sequence TSE T2 in b0					
Co-ordinate	EPI without parallel image	EPI with GRAPPA R-factor 2	EPI with mSENSE R-factor 2	EPI with GRAPPA R-factor 3	EPI with mSENSE R-factor 3
x1	0	1	1	0	0
y1	-12	-5	-3	-3	0
x2	0	-1	0	0	-0.41
y2	-14	-5	-4	-4	-0.24
x3	0	0	0	0	0
y3	-11	-5	-3	-2	0
x4	-1	0	1	1	-0.41
y4	-5	-5	1	0	0.24
x5	1	0	0	0	0
y5	-11	-4	-2	-1	0

Table 4.17 Deviation at each co-ordinate compare with sequence TSE T2 in b1000 at location C

Deviation at each co-ordinate compared with sequence TSE T2 in b1000					
Co-ordinate	EPI without parallel image	EPI with GRAPPA R-factor 2	EPI with mSENSE R-factor 2	EPI with GRAPPA R-factor 3	EPI with mSENSE R-factor 3
x1	1	1	0	0	0
y1	-12	-5	-5	-3	-5
x2	0	0	-1	0	0
y2	-14	-6	-5	-4	-5
x3	0	1	0	0	1
y3	-11	-5	-3	-2	-5
x4	-1	0	1	1	0
y4	-6	-1	-1	0	-1
x5	1	0	0	0	1
y5	-12	-4	-4	-1	-4

Table 4.18 Deviation at each co-ordinate compare with sequence TSE T2 in b0 at location D

Deviation at each co-ordinate compared with sequence TSE T2 in b0					
Co-ordinate	EPI without parallel image	EPI with GRAPPA R-factor 2	EPI with mSENSE R-factor 2	EPI with GRAPPA R-factor 3	EPI with mSENSE R-factor 3
x1	0	-1	-1	0	-1
y1	8	5	7	5	5
x2	n/a	n/a	n/a	n/a	n/a
y2	n/a	n/a	n/a	n/a	n/a
x3	0	0	-1	0	0
y3	-1	1	3	1	3
x4	0	0	0	0	0
y4	16	9	10	7	8
x5	-1	-1	0	0	-1
y5	24	14	16	10	12

Table 4.19 Deviation at each co-ordinate compare with sequence TSE T2 in b1000 at location D

Deviation at each co-ordinate compared with sequence TSE T2 in b1000					
Co-ordinate	EPI without parallel image	EPI with GRAPPA R-factor 2	EPI with mSENSE R-factor 2	EPI with GRAPPA R-factor 3	EPI with mSENSE R-factor 3
x1	0	-1	0	0	n/a
y1	8	5	8	5	n/a
x2	n/a	n/a	n/a	n/a	n/a
y2	n/a	n/a	n/a	n/a	n/a
x3	0	0	-2	0	n/a
y3	-1	0	2	1	n/a
x4	0	1	0	0	n/a
y4	16	8	11	7	n/a
x5	-1	0	0	0	n/a
y5	24	14	17	10	n/a

4.5 Percent deviation of distortion

The percent deviation of each pulse sequence was calculated as in equation

[(variation parameter – TSE T2)/TSE T2] x100

Note: Percent deviation value show in plus (+) and minus (-). These signs represent the distortion direction in plus (+) direction is up and minus (-) direction is down.

Table 4.20 Percent deviation at each co-ordinate compared with sequence TSE T2 in b0 at location B

Percent deviation at each co-ordinate compared with sequence TSE T2 in b0					
Co-ordinate	EPI without parallel image	EPI with GRAPPA R-factor 2	EPI with mSENSE R-factor 2	EPI with GRAPPA R-factor 3	EPI with mSENSE R-factor 3
x1	-0.13	-0.13	0	-0.13	-0.13
y1	-3.60	-1.20	-0.9	-0.60	0
x2	n/a	n/a	n/a	n/a	n/a
y2	n/a	n/a	n/a	n/a	n/a
x3	-0.13	0	-0.13	0	0
y3	2.40	1.20	2.10	1.20	1.80
x4	-0.13	-0.13	-0.13	0	0
y4	2.14	1.61	1.88	1.07	1.61
x5	0	0	0	0.14	0
y5	-4.50	-1.8	-1.20	-1.20	-0.60

Table 4.21 Percent deviation at each co-ordinate compared with sequence TSE T2, in b10000 at location B

Percent deviation at each co-ordinate compared with sequence TSE T2 in b1000					
Co-ordinate	EPI without parallel image	EPI with GRAPPA R-factor 2	EPI with mSENSE R-factor 2	EPI with GRAPPA R-factor 3	EPI with mSENSE R-factor 3
x1	-0.13	-0.13	-0.13	0	n/a
y1	-3.30	-1.20	-0.30	-1.2	n/a
x2	n/a	n/a	n/a	n/a	n/a
y2	n/a	n/a	n/a	n/a	n/a
x3	-0.13	0	-0.13	0	-0.25
y3	2.10	1.20	2.70	0.60	1.50
x4	-0.13	0	-0.13	0	n/a
y4	2.14	1.07	2.68	0.80	n/a
x5	0	0.14	0.14	0.28	n/a
y5	-4.50	-2.10	-0.90	-1.50	n/a

Table 4.22 Percent deviation at each co-ordinate compared with sequence TSE T2, in b0 at location C

Percent deviation at each co-ordinate compared with sequence TSE T2 in b0					
Co-ordinate	EPI without parallel image	EPI with GRAPPA R-factor 2	EPI with mSENSE R-factor 2	EPI with GRAPPA R-factor 3	EPI with mSENSE R-factor 3
x1	0	0.18	0.18	0	0
y1	-2.21	-0.92	-0.55	-0.55	0
x2	0	-0.18	0	0	-0.18
y2	-2.79	-1.00	-0.80	-0.80	-0.20
x3	0	0	0	0	0
y3	-2.03	-0.92	-0.55	-0.37	0
x4	-0.18	0	0.18	0.18	-0.18
y4	-0.86	-0.86	0.17	0	0.17
x5	0.20	0	0	0	0
y5	-2.02	-0.74	-0.37	-0.18	0

Table 4.23 Percent deviation at each co-ordinate compared with sequence TSE T2, in b1000 at location C

Percent deviation at each co-ordinate compared with sequence TSE T2 in b1000					
Co-ordinate	EPI without parallel image	EPI with GRAPPA R-factor 2	EPI with mSENSE R-factor 2	EPI with GRAPPA R-factor 3	EPI with mSENSE R-factor 3
x1	0.18	0.18	0	0	0
y1	-2.21	-0.92	-0.92	-0.55	-0.92
x2	0	0	-0.18	0	0
y2	-2.79	-1.20	-1.00	-0.80	-1.00
x3	0	0.17	0	0	0.17
y3	-2.03	-0.92	-0.55	-0.37	-0.92
x4	0.18	0	0.18	0.18	0
y4	-1.03	-0.17	-0.17	0	-0.17
x5	0.20	0	0	0	0.20
y5	-2.21	-0.74	-0.74	-0.18	-0.74

Table 4.24 Percent deviation at each co-ordinate compared with sequence TSE T2, in b0 at location D

Percent deviation at each co-ordinate compared with sequence TSE T2 in b0					
Co-ordinate	EPI without parallel image	EPI with GRAPPA R-factor 2	EPI with mSENSE R-factor 2	EPI with GRAPPA R-factor 3	EPI with mSENSE R-factor 3
x1	0	-0.29	-0.29	0	-0.29
y1	2.32	1.45	2.03	1.45	1.45
x2	n/a	n/a	n/a	n/a	n/a
y2	n/a	n/a	n/a	n/a	n/a
x3	0	0	-0.26	0	0
y3	-0.29	0.29	0.87	0.29	0.87
x4	0	0	0	0	0
y4	4.16	2.34	2.60	1.82	2.08
x5	0	-0.32	0	0	-0.32
y5	7.25	4.06	4.64	2.90	3.48

Table 4.25 Percent deviation at each co-ordinate compared with sequence TSE T2, in b1000 at location D

Percent deviation at each co-ordinate compared with sequence TSE T2 in b1000					
Co-ordinate	EPI without parallel image	EPI with GRAPPA R-factor 2	EPI with mSENSE R-factor 2	EPI with GRAPPA R-factor 3	EPI with mSENSE R-factor 3
x1	0	-0.29	0	0	n/a
y1	2.32	1.45	2.32	1.45	n/a
x2	n/a	n/a	n/a	n/a	n/a
y2	n/a	n/a	n/a	n/a	n/a
x3	0	0	-0.51	0	n/a
y3	-0.29	0	0.58	0.29	n/a
x4	0	0.29	0	0	n/a
y4	4.16	2.08	2.86	1.82	n/a
x5	-0.32	0	0	0	n/a
y5	6.96	4.06	4.93	2.90	n/a

CHAPTER V
DISCUSSION AND CONCLUSION

5.1 Discussion

Diffusion Weighted Imaging (DWI) is a technique in MRI to detect low diffusion, appear in bright region, mostly used in case of stroke, brain tumor, and brain metastasis. In general, Echo Planar Imaging (EPI) is chosen with the major problem of geometric distortion at susceptibility area such as base of skull.

In this in vitro study, EPI with and without parallel image (mSENSE and GRAPPA) had been applied in phantom study and the result images were compared with TSE T2, the gold standard technique to reduce distortion artifact at base of skull.

Table 5.1 shows that the best parameter to reduce distortion is EPI with GRAPPA R-factor 3 because GRAPPA is based on a variable density of modified image reconstruction in the k-space (before Fourier transform). It exploits the sensitivity profiles of each element of coil array. First, MRI signal data is acquired simultaneously from each individual component of the coil array. Next, the signal data for each individual component is linearly combined to produce spatial harmonics that are used to create several k-space lines acquired in the center of the k-space. The central calibration lines are acquired during the entire acquisition and are added to the whole k-space acquisition. This matrix is Fourier-transformed to produce the final image. Our result in reduce distortion is the same as Blaimer et al(14)., as GRAPPA has proven to be well suited for EPI. In almost every area tested so far, GRAPPA showed reconstructions without modifying either the EPI sequence or the reconstruction algorithm. Bhagat et al(17). studied in 1.5 Tesla and scan parameter such as Repetition Time (TR), Echo Time (TE) were the same as this study, but they used different matrix size of 96x128, which showed that the reviewer's score the GRAPPA and mSENSE R-factor=2 images were shaper than EPI without parallel image. In image acquired with higher acceleration factor (R-factor=3, 4) it suffered from pernicious reconstruction artifacts, such as aliasing and structural noise enhancement.

The image distortion is determined from the maximum percent deviation in EPI without parallel image in both b0 and b1000 at location B and D, because this is close to susceptibility area. The direction of distortion, an undefined cause as EPI is basic concept from k-space point ,blipping and gradient flip In EPI with GRAPPA and mSENSE R-factor 2 the maximum percent deviation is similar.

Table 5. 1 Maximum percent deviation at each co-ordinate compare with TSE T2 EPI without parallel image, EPI with GRAPPA R-factor 2, 3 and EPI with mSENSE R-factor 2, 3

Location	b-value	Position	Maximum percent deviation				
			EPI without parallel image	EPI with GRAPPA R-factor 2	EPI with GRAPPA R-factor 3	EPI with mSENSE R-factor 2	EPI with mSENSE R-factor 3
B	b0	y5	4.5	1.8	1.2	2.1	1.8
B	b1000	y5	4.5	2.1	1.5	2.7	1.5
C	b0	y2	2.8	<1	<1	<1	<1
C	b1000	y2	2.8	1.2	<1	<1	<1
D	b0	y5	-7.25	-4.06	-2.9	-4.64	-3.5
D	b1000	y5	-6.96	-4.06	-2.9	-4.93	n/a

*note in sign (+) represent distortion direction is down and (-) distortion direction is up

From figure 5.1 in EPI with mSENSE R-factor 3 and table 5.2 the object is unable to measure because mSENSE technique is a modified image reconstruction in the image space, with an array of parallel receivers; mSENSE reconstruction reduces the number of Fourier encoding steps. Ruel et al. found mSENSE reconstruction performed for each coil by increasing the distance between sampling line in k-space. This result, after Fourier transform, in reduce field of view yield aliasing image. Blaimer et al. reported image reconstruction of single-shot EPI applications with SENSE is problematic because the distortions in EPI images and coil sensitivity maps are different. This means that the image intensity given location may not be corresponded to the correct value in the sensitivity map. Possible solutions have been reported to overcome this problem with SENSE.

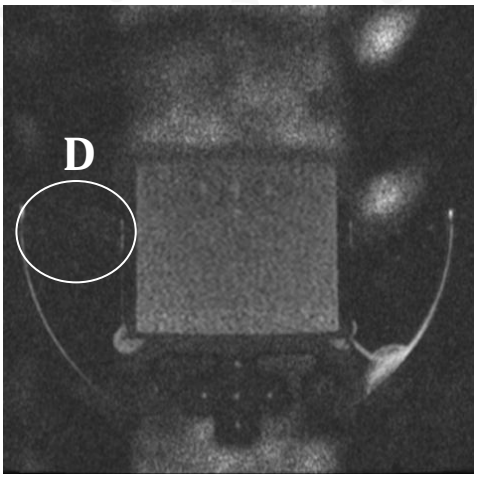

Figure 5.1 EPI with mSENSE R-factor 3

Table 5. 2 Percent deviation of co-ordinate(x,y) in sequence TSE T2,EPI with mSENSE R-factor 3 in b1000 at location D

Position	Co-ordinate TSE T2	Co-ordinate b1000	Percent deviation
x1	348	n/a	n/a
y1	345	n/a	n/a
x2	348	n/a	n/a
y2	308	n/a	n/a
x3	389	n/a	n/a
y3	345	n/a	n/a
x4	349	n/a	n/a
y4	385	n/a	n/a
x5	308	n/a	n/a
y5	345	n/a	n/a

Table 5.3 demonstrates the maximum percent deviation of EPI with GRAPPA R-factor 2 and 3. When R-factor increases, the phase-encoding decreases from basic of EPI. More phase encoding produces more distortion. Distortion decreased as shown in percent deviation in table 5.3.

Table 5.3 Maximum percent deviation at each co-ordinate compare with sequence TSE T2, EPI with GRAPPA R-factor 2and EPI with GRAPPA R-factor 3 in b0 and b1000

Location	b-value	Position	Maximum percent deviation	
			EPI with GRAPPA R-factor 2	EPI with GRAPPA R-factor 3
B	b0	y5	1.8	1.2
B	b1000	y5	2.1	1.5
C	b0	y2	<1	<1
C	b1000	y2	1.2	<1
D	b0	y5	-4.06	-2.9
D	b1000	y5	-4.06	-2.9

*note in sign (+) represent distortion direction is down and (-) distortion direction is up

In clinical applications the parameter EPI with GRAPPA R-factor 3 could be implemented in clinical studies to reduce distortion image at base of skull.

5.2 Conclusion

In Diffusion Weighted Imaging using Echo Planar Imaging in MRI 1.5 Tesla at susceptibility area by using Magphan phantom, EPI with GRAPPA R-factor 3 is the best parameter suited for reduce distortion because GRAPPA is k-space based, method that calculate missing k-space lines before Fourier transformation of the raw data, it could improve image distortion.

REFERENCES

1. Rinck, P. Magnetic Resonance in Medicine The Basic Textbook of the European Magnetic Resonance Forum [Online]. 2013. Available from: www.magnetic-resonance.org
2. Lansberg, M. G.Norbash, A. M.Marks, M. P.Tong, D. C.Moseley, M. E.and Albers, G. W. Advantages of Adding Diffusion-Weighted Magnetic Resonance Imaging to Conventional Magnetic Resonance Imaging for Evaluating Acute Stroke. Arch Neurol 57 (2000): 1311-6.
3. Roland, B. Basic principles of diffusion-weighted imaging. Eur J Radiol 45 (2003): 169-84.
4. Lin, F. H.and Tsai, S. Y. Parallel Magnetic Resonance Imaging Acquisition and Reconstruction: Application to functional and Spectroscopic Imaging in Human Brain. In Hayat, M. A. (eds), Methods of Cancer Diagnosis, Therapy, and Prognosis, 245-62. Place: Published: Springer Netherlands; 2011 Number of 245-62. p.
5. McRobbie, D. W.Moore, E. A.Graves, M. J.and Prince, M. R. MRI from The Picture to Proton, Diffusion Imaging. 2nd ed. Place: Published: Cambridge University Press; 2006.
6. Liney, G. P. Magnetic Resonance Imaging (MRI).Introduction. [Online]. 2011. Available from: http://www.hull.ac.uk/mri/lectures/gpl_page.html
7. Puddephat, M. Magnetic Resonance Imaging.Principle of Magnetic Resonance Imaging. [Online]. 2010. Available from: http://www.mikepuddephat.com/Page/1603/Principles-of-magnetic-resonance-imaging [2013, Dec.]
8. Jones, J.and Bashir, U. MRI physic.Relaxation. [Online]. 2014. Available from: http://radiopaedia.org/articles/relaxation [2013, Nov.]
9. Blink, E. J. Basic MRI physics Relaxation [Online]. 2004. Available from: http://www.mri-physics.net/textuk.html [2013, Nov.]
10. Brown, M. A.and Semelka, R. C. MRImaging Abbreviations,Definitions, and Descriptions:A Review. Radiology 213 (1999): 647–62.
11. Wang, J. MRI Resonance Imaging.MRI Radio Frequency Coils. [Online]. 2010. Available from: https://wiki.engr.illinois.edu/display/BIOE414/Team+4+-+MRI+Radio+Frequency+Coils [2013, Dec.]
12. Hornak, J. P. Magnetic Resonance Imaging.Imaging Hardware. [Online]. 2000. Available from: http://www.cis.rit.edu/class/schp730/lect/lect-17.htm [2013, Dec]
13. Mudgal, P.and Y., W. MRI Physics.MRI artifacts. [Online]. 2014. Available from: http://radiopaedia.org/articles/mri-artifacts

14. Blaimer, M.Breuer, F.Mueller, M.Heidemann, R. M.Griswold, M. A.and Jakob, P. M. SMASH, SENSE, PILS, GRAPPA How to Choose the Optimal Method. Top Magn Reson Imaging 15 (2004): 223–36.
15. DeLaPaz, R. L. Echo planar imaging. RadioGraphics 14 (1994): 1045-58.
16. Clark, G. D. Advance in Magnetic Resonance Imaging. In Clark, G. D. (eds): AAPM/ISEP Diagnostic Imaging Workshop2013.
17. Bhagat, Y. A.Naik, S. H.and Beaulieu, C. F. Comparison of Generalized Autocalibrating Partially Parallel Acquisitions and Modified Sensitivity Encoding for Diffusion Tensor Imaging. AJNR Am J Neuroradiol 28 (2007): 293–98.
18. ACR. ACR Phantom Test Guidance, ACR MRI Accreditation Program. Place: Published2004. 1-22. p.

APPENDICES

Appendix A: Case record form

Table 6.1 Pulse sequence acquisition parameters

Pulse sequence	TR (msec)	TE (msec)	FOV (mm)	Slice thickness (mm)	Slice gap (mm)	Matrix	Scan time
TSE T2		171	230x230	2	0	256x256	
EPI without parallel image		171	230x230	2	0	200x200	
EPI with mSENSE 2		171	230x230	2	0	200x200	
EPI with mSENSE 3		171	230x230	2	0	200x200	
EPI with GRAPPA 2		171	230x230	2	0	200x200	
EPI with GRAPPA 3		171	230x230	2	0	200x200	

Co-ordinate position in all pulse sequences

Table 6.2 Pulse sequence and scan number (#)

Location										
Object number	1		2		3		4		5	
Co-ordinate	x	y	x	y	x	y	x	y	x	y
Co-ordinate point										

Deviation of distortion co-ordinate in each sequence

Table 6. 3 Deviation at each co-ordinate compare with sequence TSE T2 in b-value (b0, b1000) at location___

Deviation at each co-ordinate compared with sequence TSE T2 in b-value					
Co-ordinate	EPI without parallel image	EPI with GRAPPA R-factor 2	EPI with mSENSE R-factor 2	EPI with GRAPPA R-factor 3	EPI with mSENSE R-factor 3
x1					
y1					
x2					
y2					
x3					
y3					
x4					
y4					
x5					
y5					

Percent deviation of distortion co-ordinate in each sequence

Table 6. 4 Percent deviation at each co-ordinate compared with sequence TSE T2 in b-value (b0, b1000) at location___

Percent deviation at each co-ordinate compared with sequence TSE T2 in b-value					
Co-ordinate	EPI without parallel image	EPI with GRAPPA R-factor 2	EPI with mSENSE R-factor 2	EPI with GRAPPA R-factor 3	EPI with mSENSE R-factor 3
x1					
y1					
x2					
y2					
x3					
y3					
x4					
y4					
x5					
y5					

Appendix B: Quality control of MRI systems

Site: King Chulalongkorn Memorial Hospital **Date:** 07/06/2013

Equipment:

MRI System Manufacturer: Siemens

Model: Magnetom 1.5 Tesla

QC Phantom: ACR Phantom

Serial number: J10477

Made in U.S.A

Quality of MRI system consists of seven contents (18)

- Geometric accuracy
- Slice thickness accuracy
- Slice position accuracy
- Image intensity uniformity
- Percent signal ghosting
- High contrast spatial resolution
- Low contrast object detectability

Procedures the QC Phantom

Place the QC phantom on the head coil, and level it. Turn “NOSE” side to tilt the top of phantom and turn “CHIN” side away from the gantry. Use the laser alignment lights to position the phantom.

The MRI accreditation program requires the acquisition of a sagittal localizer and four axial series of images. The same set of eleven slice locations within the phantom is required using the scanner’s head coil. The scan parameters for the localizer and the first two axial series of imaged are fully prescribed by ACR in the scanning instructions as the ACR sequence or ACR images. The third and fourth series of axial images based on King Chulalongkorn Memorial hospital is the spin echo T1 and T2 protocols and are referred to set the sequences or site

images. To discuss the image data it is convenient to introduce name for the different sets of image and numbering for the slice locations within the phantom.

The localizer is a 20 mm thick single slice spin echo acquisition through the center of phantom, and is referred to simply as the localizer.

The first axial series is a spin echo acquisition with ACR specified scan parameters that are typical of T1-weighted acquisitions. This series is called the ACR T1 series.

The second axial series is a double spin echo acquisitions with ACR specified scan parameters that are typical of proton density/T2-weighted acquisitions. When analyzing data from this acquisition only the second-echo image are used. The set of second-echo image from this acquisition is called the ACR T2 series.

The third and fourth axial series are based on the scan parameters at King Chulalongkorn Memorial Hospital normally used its clinical protocols for axial head T1and head T2 weighting. These series are called the clinical T1 and T2.

For ACR axial T1 and T2 series require slice thickness at 5 mm and the gap at 5 mm thus, the set of eleven slices scan distance from center of first slice to center of last slice is 100 mm.

Table 7.1 ACR Pulse sequence Acquisition parameters

Study	Pulse Sequence	TR (ms)	TE (ms)	FOV (cm)	No. of slices	Slice Thick. (mm)	Slice Gap (mm)	NEX	Matrix	Receive Band Width (kHz)	Scan Time (min:sec)
ACR Sagittal locator	Spin Echo	200	20	25	1	20	N/A	1	256 256	201	0:53
ACR Axial T1	Spin Echo	500	20	25	11	5	5	1	256 256	150	2:07
ACR Axial T2 Double echo	Spin Echo	2000	20/80	25	11	5	5	1	256 256	100	8:36

Table 7.2 Clinical Pulse sequence Acquisition parameters

Study	Pulse Sequence	TR (ms)	TE (ms)	FOV (cm)	No. of slices	Slice Thick. (mm)	Slice Gap (mm)	NEX	Matrix	Receive Band Width (kHz)	Scan Time (min:sec)
Clinical Axial T1 weighted	Spin Echo	550	8.9	Freq: 23 Phase: 20.1	20	5	1	1	384 270	150	2:27
Clinical Axial T2 weighted	Turbo Spin Echo	4700	96	Freq: 23 Phase: 20.1	20	5	1	2	448 326	190	2:25

7.1 Geometric Accuracy

Purpose: To assess the accuracy of the image lengths in the imaged subject. A failure means that dimensions in the images differ from the true dimensions substantially more than ± 2 mm.

Method: 1. Display the localizer, measure the end-to-end length of the phantom as it appears in the localizer (line No.1).

2. Display slice 1 of the ACR T1 series. Measure the diameter of the phantom in 2 directions: top-to-bottom (line No.2) and left-to-right (line No.3).

3. Display slice 5 of the ACR T1 series. Measure the diameter of the phantom in 4 directions: top-to-bottom (line No.4), left-to-right (line No.5), and both diagonals (line No.6 and 7).

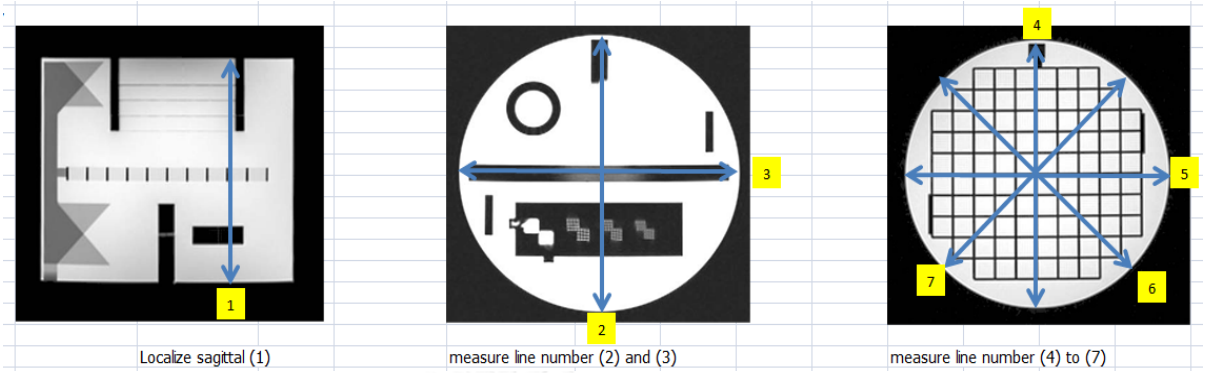

Figure 7.1 Geometric accuracy

Table 7.3 Result Geometric accuracy

Line No.	True Value (mm)	Sagittal Locator		ACR T1		ACR T2 TE 20		ACR T2 TE 80	
		Meas. (mm)	Differ. (mm)	Meas. (mm)	Differ (mm)	Meas. (mm)	Differ (mm)	Meas. (mm)	Differ. (mm)
1	148	148.31	0.31	-	-	-	-	-	-
2	190	-	-	190.11	0.11	190.15	0.15	189.45	1.45
3	190	-	-	191.06	0.06	191.59	0.59	191.36	1.36
4	190	-	-	190.89	0.89	191.34	1.34	190.40	0.40
5	190	-	-	191.12	1.12	190.90	0.90	190.88	0.88
6	190	-	-	191.45	1.45	190.27	0.27	190.09	0.09
7	190	-	-	191.12	1.12	190.77	0.77	190.64	0.64

Recommended Action Criteria: All measured dimension should be within ±2 mm of their true values.

PASS

7.2 Slice thickness accuracy

Purpose: To assess the accuracy of a slice of specified thickness. The prescribed slice thickness is compared with the measured slice thickness.

Method: For slice thickness accuracy the lengths of 2 signal ramps in slice 1 are measured. This is done for both ACR series. The ramps appear in a structure called the slice thickness insert. The 2 ramps are crossed: one has a negative slope and the other a positive slope with respect to the plane of slice 1. They are produced by cutting 1 mm wide slots in a block of plastic. The slots are open to the interior of the phantom and are filled with the same solution that fills the bulk of the phantom. The signal ramps have a slope of 10 to 1 with respect

to the plane of slice 1, that is they make an angle of about 5.71° with slice 1. Therefore, the signal ramps will appear in the image of slice 1 with a length that is 10 times the thickness of the slice. If the phantom is tilted in the right-left direction, one ramp will appear longer than the other. Having crossed ramps allows for correction of the error introduced by right-left tilt.

For each ACR series, the length of the signal ramps in slice 1 is measured according to the following procedure:

1. Display slice 1, and magnify the image by a factor of2 to 4. Adjust the display level so that the signal ramps are well visualized. The ramp signal is much lower than surrounding water.

2. Place a rectangular ROI at the middle of each signal ramp as shown in Figure 2. Note the mean signal values for each of these 2 ROIs then average those 2 values together. The result is a number approximating the mean signal in the middle of the ramps.

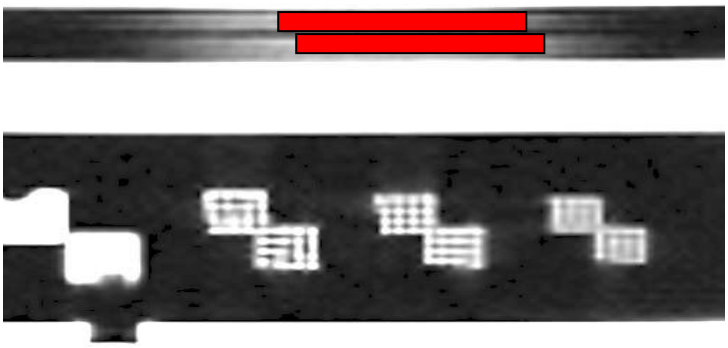

Figure 7.2 ROIs placed for measuring average signal in the ramps.

3 Display level to half of the average ramp signal calculated. Use the on-screen length measurement tool of the display station to measure the lengths of the top and bottom ramps. Record these lengths.

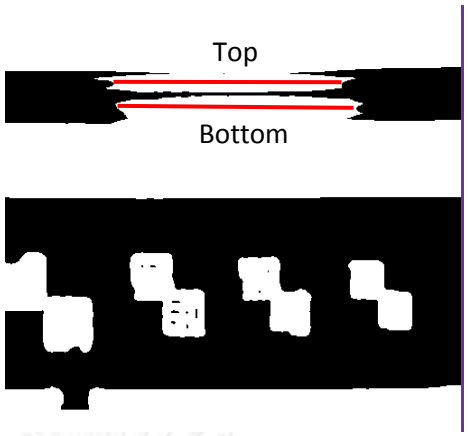

Figure 7.3 Magnified region of slice 1 showing slice thickness signal ramps

The display window is zero and the level is half the average signal level of the ramps. The length measurements for the ramps are shown on the image.

The slice thickness is calculated using the following formula

Slice thickness = 0.2 x (top x bottom)/(top + bottom)

Table 7.4 Result slice thickness accuracy

Series	Slice thickness Set(mm)	Slice thickness Measurement(mm)	Results
ACR T1	5	5	PASS
ACR T2 TE 20	5	5.2	PASS
ACR T2 TE 80	5	5	PASS

Recommended Action Criteria: For ACR series the measured thickness should be 5.0 ±0.7mm

7.3 Slice Position Accuracy

Purpose: To assesses the accuracy with which slices can be prescribed at specific locations utilizing the localizer image for positional reference.

Method: Slice position accuracy test the differences between the prescribed and actual positions of slices 1 and 11 are measured. These measurements are made for the ACR T1 and T2 series. The slices 1 and 11 are prescribed so as to be aligned with the vertices of the crossed 45° wedges at the inferior and superior ends of the phantom respectively. On slices 1 and 11 the

crossed wedges appear as a pair of adjacent, dark, vertical bars at the top (anterior side) of the phantom. For both slice 1 and slice 11, if the slice is exactly aligned with the vertex of the crossed wedges, then the wedges will appear as dark bars of equal length on the image. By design of the wedges, if the slice is displaced superiorly with respect to the vertex, the bar on the observer's right (anatomical left) will be longer. If the slice is displaced inferiorly with respect to the vertex, the bar on the left will be longer.

Measurements are made for slices 1 and 11 of the ACR T1 and ACR T2 series. Use the following procedure for each image:

1. Display the slice. Magnify the image by a factor of 2 to 4, keeping the vertical bars of the crossed wedges within the displayed portion of the magnified image.

2. Adjust the display window so the ends of the vertical bars are well defined Use the on-screen length measurement tool to measure the difference in length between the left and right bars. The length to measure is indicated by the arrows in Figure 7.5

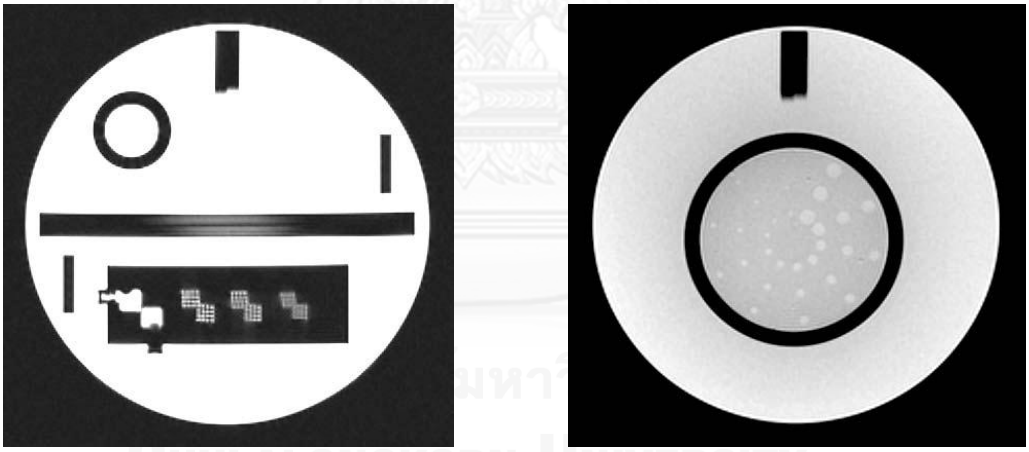

Figure 7.4 Images of slice 1 (left) and slice 11 (right) with the pairs of vertical bars from the 45° crossed wedges indicated.

On these images the length difference between the right and left bars is small and typical of well-positioned slices.

Figure 7.5 Images of slice 1 illustrating measurement of slice position error. The arrows indicate the bar length difference measurement that is to be made.

(left) The bar on the right is longer, meaning the slice is mispositioned superiorly; this bar length difference is assigned a positive value(+).

(right) The bar on the left is longer, meaning the slice is mispositioned inferiorly; this bar length difference is assigned a negative value(-).

Table 7.5 Result from slice position 1 and 11 ACR phantom.

Series	ACR T1	ACR T2 TE 20	ACR T2 TE80	Results
Slice location:1	+1	+1	+1	PASS
Slice location:11	-3.28	-2.14	-2.38	PASS

Recommended Action Criteria: The magnitude of each bar length difference should be less or equal to 5mm.

7.4 Image Intensity Uniformity: Percent integral Uniformity (PIU)

Purpose: To measures the uniformity of the image intensity over a large water-only region of the phantom lying near the middle of the imaged volume and thus near the middle of the head coil

Method: Display slice location 7. Place a large, circular region-of-interest (ROI) on image. This ROI should have an area of between 195 cm^2 and 205 $cm^{2.}$. Set the display window to its minimum, and lower the level until the entire area inside the large ROI is white. Place the small ROI roughly 1 cm^2 at the region of dark pixels develops inside the large ROI. Record the mean pixel value for this 1 cm^2 ROI. This is the measured low-signal value. Raise the level until all but a small, roughly

1 cm^2 region of white pixels remains inside the large ROI. This is the region of highest signal. Record the average pixel value for this 1 cm^2 ROI. This is the measured high-signal value.

Figure 7.6 (right) ROI placement for low signal-value, (left) ROI placement for HIGH signal-value.

The measured high- and low-signal values for each of the ACR series are combined to produce a value called **percent integral uniformity** (PIU). Use the following formula to calculate PIU:

$$\mathbf{PIU = 100 \times (1 - \{ (high - low)/(high + low) \}).}$$

Table 7.6 Result Image intensity uniformity

	Low signal	High signal	PIU (%)	Result
ACR Axial T1	1440	1454.21	99.51	PASS
ACR Axial T2 TE 20	1503.47	1519.08	99.40	PASS
ACR Axial T2 TE 80	823.27	835.15	99.28	PASS

Recommended Action Criteria: PIU should be greater than or equal to 87.5% for MRI systems with field strengths less than 3 Tesla.

7.5 Percent signal ghosting

Purpose: To assesses the level of ghosting in the image.

Method: Percent signal ghosting measurements are made on slice 7 of the ACR T1 series. Using the workstation's ROI tool, 5 intensity measurements are made: the average intensity in the primary image of the phantom, and the average intensity in the background at 4 locations outside of the phantom. The value for the ghosting, as a fraction of the primary signal, is calculated using the following formula:

$$\text{Ghosting ratio} = \left| \left((\text{top} + \text{btm}) - (\text{left} + \text{right}) \right) / \left(2 \times (\text{large ROI}) \right) \right|$$

Where top, bottom, left, right, and large ROI are the average pixel values for the ROIs of the same names. The vertical bars enclosing the right-hand side of the equation mean to take the magnitude of the enclosed value.

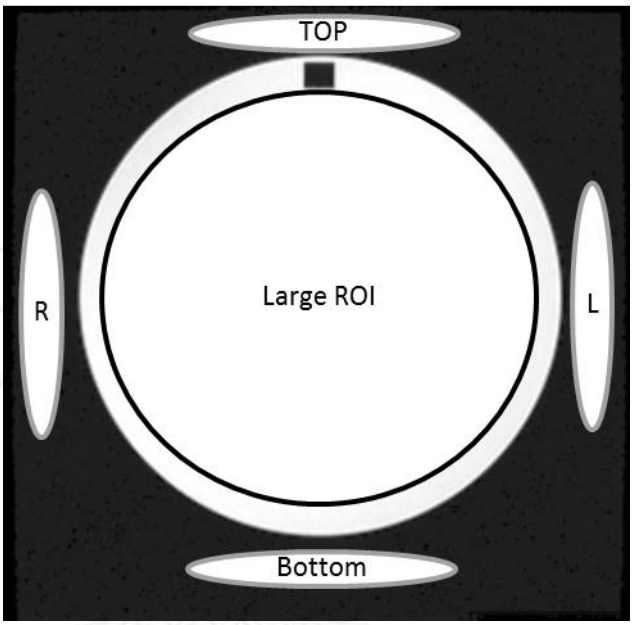

Figure 7.7 ROI to measure pixel value for Percent signal ghosting

Table 7.7 Pixel value and Result Percent signal ghosting

	Top	Bottom	Left	Right	Large ROI	Calculated value	Result
ACR T1	11.96	10.68	8.25	9.24	1430.04	0.0018	PASS
ACR T2 TE 20	13.87	11.41	11.24	8.74	1491.17	0.0017	PASS
ACR T2 TE 80	10.11	11.09	6.11	5.67	808.65	0.0058	PASS

Recommended Action Criteria: The ghosting ratio should be less than or equal to 0.025.

7.6 High Contrast Spatial Resolution

Purpose: To assess the scanner's ability to resolve small objects when the contrast-to-noise ratio is sufficiently high.

Method: Display the slice 1 ACR axial series, Magnify the image by a factor of between 2 and 4, Look at the rows of hole in the UL (Upper Left) array, and adjust the display window and level to best show the holes as distinct from one another, score the image as resolved right to left at this particular hole size. Look at the holes in the LR (lower right) array and adjust the display window and level to best show the holes as distinct from one another. Make a note of the smallest hole size resolved in each direction

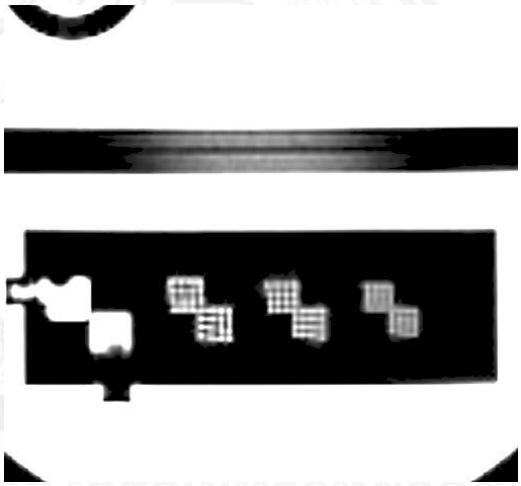

Figure 7.8 Magnified portion of slice 1 displayed appropriately for visually assessing high contrast resolution.

Table 7.8 Result high contrast spatial resolution

	Spatial resolution	Result
ACR Axial T1	1.0 mm	PASS
ACR Axial T2 TE 20	1.0 mm	PASS
ACR Axial T2 TE 80	1.0 mm	PASS

Recommended Action Criteria: the measured resolution should be 1.0 mm or better.

7.7 Low contrast object Detectability

Purpose: To assesses the extent to which objects of low contrast are discernible in the images

Method: Measurements are made for the ACR and clinical series. The low-contrast objects appear on 4 slices: slices 8 through 11. In each slice the low-contrast objects appear as rows of small disks, with the rows radiating from the center of a circle like spokes in a wheel. Each spoke is made up of three disks, and there are ten spokes in each circle. All the disks on a given slice have the same level of contrast. In order, from slice 8 to slice 11, the contrast values are 1.4%, 2.5%, 3.6%, and 5.1%. All the disks in a given spoke have the same diameter. Starting at the 12 o'clock position and moving clockwise, the disk diameter decreases progressively from 7.0 mm at the first spoke to 1.5 mm at the tenth spoke. The measurements for this test consist of counting the number of complete spokes seen in each of the four slices. This is done for each of the four axial series.

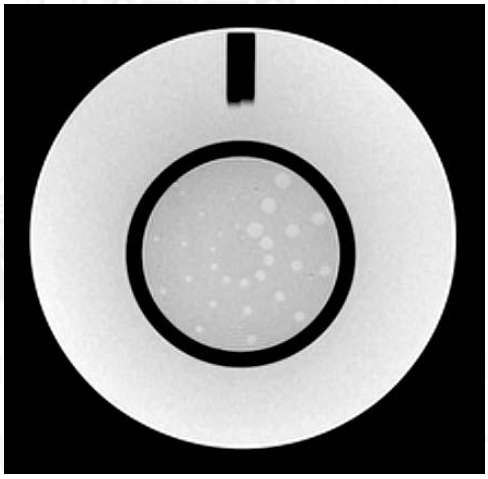

Figure 7.9 Image of slice 11 showing the circle of low contrast objects for the low-contrast object detectability test

Table 7.9 Result low contrast detectability

	Number of spoke					
Contrast value	1.40%	2.50%	3.60%	5.10%	Total	Result
ACR T1	5	9	9	10	33	PASS
ACR T2 TE 20	6	10	10	10	36	PASS
ACR T2 TE 80	3	10	10	10	33	PASS
Clinical T1	2	5	9	10	26	PASS
Clinical T2	2	5	8	9	24	PASS

Recommended Action Criteria: For both in the ACR series and clinical series should have a total score of at least 9 spokes for MRI systems with field strengths less than 3 Tesla.

VITA

Name	Miss Kanokvalee Ponkanist
Date of birth	July 30, 1982
Place of birth	Bangkok,Thailand
Education	Bachelor of Science in Radiology Technology program Faculty of Science Ramkhamhaeng University, 2009
Work Experience	2003-Present Radiologic Technologist,King Chulalongkorn Memorial Hospital, Bangkok
Regional Congress	The 13th Asia-Oceania Congress or Medical Physic&11th South-East Asian Congress of Medical Physics, on December12-14, 2013, Singapore
Publication	PonkanistK.,KrisanachindaA.,LerdlumS.andKhamwanK. Appropriatetechniqueforreducedistortionindiffusion Weighted imaging MRI 1.5T. In proceedings of The 13th Asia-Oceania Congress or Medical Physic & 11th South East Asian Congress of Medical East Asian Congress of Medical Physic,121-124 pp. 12-14 December Singapore,2013.
Address	39 Soi Phahonyothin 32, Phahonyothin Road, Jatujak Ladyao Bangkok 10900